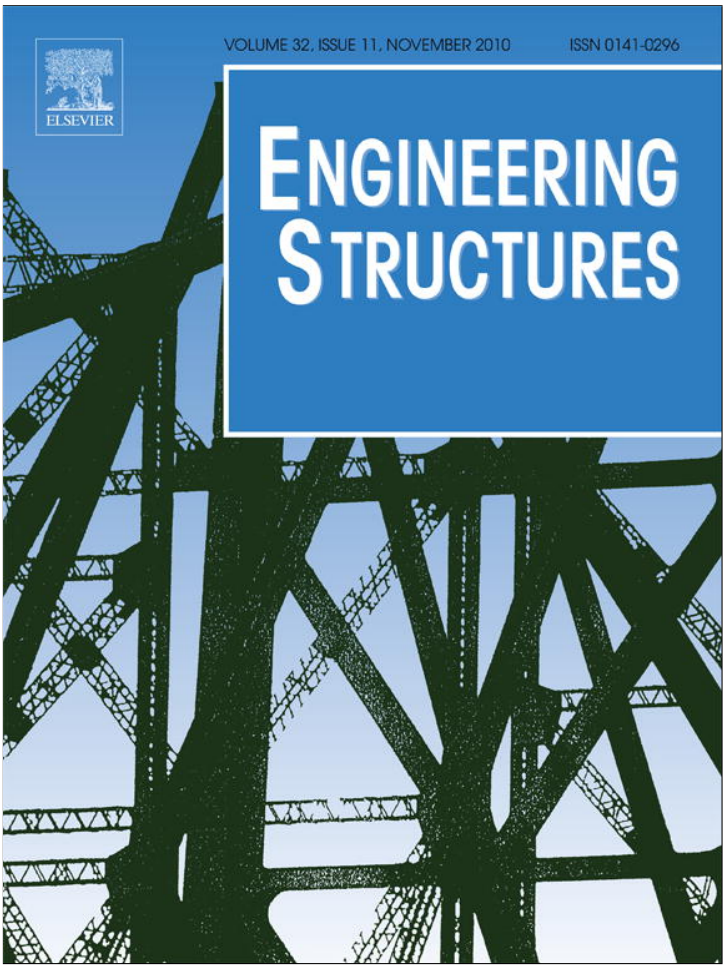

Engineering Structures 32 (2010) 3734–3757

Contents lists available at ScienceDirect

Engineering Structures

journal homepage: www.elsevier.com/locate/engstruct

Computerised interaction diagrams and moment capacity contours for composite steel–concrete cross-sections

C.G. Chiorean *

Faculty of Civil Engineering, Technical University of Cluj-Napoca, 15 C Daicoviciu Str., 400020, Cluj-Napoca, Romania

ARTICLE INFO

Article history:
Received 1 October 2009
Received in revised form
15 July 2010
Accepted 9 August 2010
Available online 16 September 2010

Keywords:
Interaction diagrams
Composite cross-sections
Ultimate strength analysis
Arc-length method
Fully yield surfaces
Biaxial bending

ABSTRACT

A new incremental-iterative procedure based on the arc-length constraint equation is proposed in order to determine both interaction diagrams and moment capacity contours for composite steel–concrete cross-sections. This procedure adopts a tangent stiffness strategy for the solution of the nonlinear equilibrium equations thus resulting in a high rate of convergence. The proposed approach has been found to be very stable for all cases examined herein even when the section is close to the state of pure compression or tension or when there are multiple solutions, and it is not sensitive to the initial or starting values, to how the origin of the reference loading axes is chosen and to the strain softening exhibited by concrete in compression. Furthermore, the proposed method can be applied to provide directly the ultimate resistances of the cross-section, in the hypothesis that one or two components of the section forces are known, without the need of knowing in advance the whole interaction diagram or moment capacity contour. An object oriented computer program with full graphical interface was developed, aimed at obtaining the ultimate strength of composite cross-sections under combined biaxial bending and axial load. In order to illustrate the proposed method and its accuracy and efficiency, this program was used to study several representative examples, which have been studied previously by other researchers using independent fiber element solutions. The examples and the comparisons made prove the effectiveness and time saving of the proposed method of analysis.

1. Introduction

The inelastic response of cross-sections under axial load and biaxial bending moments can be represented by either moment–curvature diagrams for fixed values of axial force (M–N–ϕ) or interaction diagrams that express, at failure, the interaction between the axial load and bending moments about major and minor principal axes of the cross-section. Although the moment–curvature analysis can provide useful information regarding gradual yielding, load-carrying capacity and failure mode of the cross-sections, in practice, it is sometimes desirable to have methods for calculating directly the axial force and bending moments associated with a strain distribution characterizing the failure of the cross-section. Such interaction diagrams are commonly used for the design of reinforced-concrete and composite (concrete–steel) structures. On the other hand, reliable, robust and fast inelastic analysis algorithms of the cross-sections are, for instance, essential in advanced analysis methodologies that involve accurate predictions of inelastic limit states up to or beyond structural collapse. Such algorithms, as described in the current paper, have practical value in the advanced nonlinear inelastic analysis of frameworks where elasto-plastic behaviour is modelled accounting for spread-of-plasticity effects in sections and along the element length [1,2].

In recent years, some methods have been presented for the ultimate strength analysis of various concrete and composite steel–concrete sections such as rectangular, L and T shapes, polygonal and circular, under biaxial moments and axial loads [3–13]. Among several existing techniques, two are the most common; the first consists of a direct generation of points of the failure surface by varying the position and inclination of the neutral axis (angle θ in Fig. 1) and imposing a strain distribution corresponding to a failure condition. This technique generates the failure surface through three-dimensional curves (Fig. 1), making the application of this technique rather cumbersome for practical applications. In practice, if the designer desires to check a given design, only a single plane interaction curve needs to be determined and plotted, making sure that the point defined by the applied axial load and the total applied moment falls inside the obtained plane interaction curve. The second approach is based upon the solution of the nonlinear equilibrium equations according to the classical Newton's scheme consisting of an iterative sequence of linear predictions and nonlinear corrections to obtain either the strain distribution or the location and inclination of the neutral axis which

* Tel.: +40 264 594967; fax: +40 264 594967.
E-mail address: cosmin.chiorean@mecon.utcluj.ro.

0141-0296/$ – see front matter © 2010 Elsevier Ltd. All rights reserved.
doi:10.1016/j.engstruct.2010.08.019

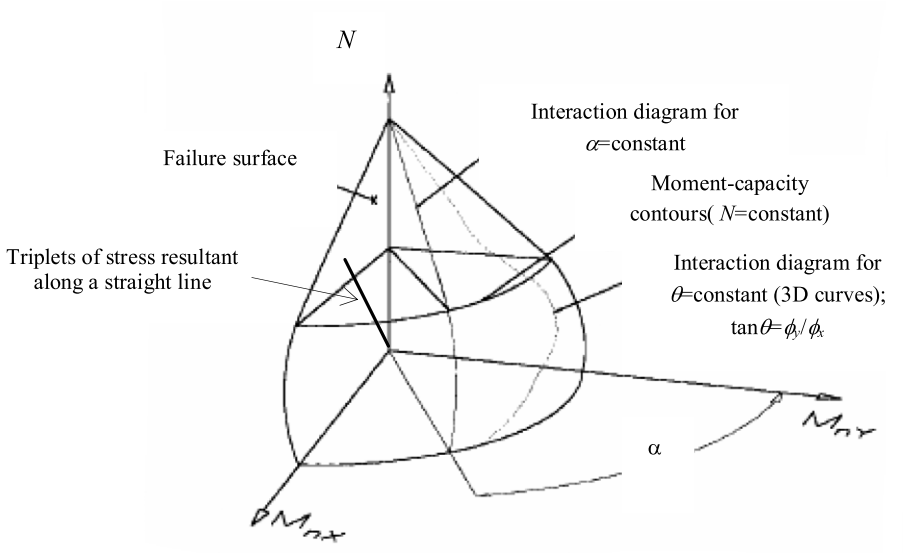

Fig. 1. Failure surface and interaction diagrams.

determines the ultimate load, where one or two components of the section forces can remain constant. In general, these methods generate plane interaction curves and give fast solutions but are sensitive to the origin of the loading axes and some problems in convergence may arise, particularly when the initial or starting values of the variables are not selected properly and under large axial forces [7]. These methods can be further distinguished by how they plot the interaction curves.

These curves may be computed, indirectly, by explicit computation of the moment–curvature response, and the failure of the cross-section corresponds to the peak of the moment–curvature diagram when any of the materials reaches its predefined maximum allowable compressive or tensile strain [8,13]. This method can be used under any loading mode, but is rather time consuming and the basic equations of equilibrium are not always satisfied [8]. On the other hand, to determine directly the interaction diagrams or load contours, the exact location of the neutral axis may be determined by solving three coupled nonlinear systems of equations by an iterative approach [5,7]. These algorithms are not straightforward to implement, starting or initial values (i.e. the location and inclination of the neutral axis) are not always simple to choose making the application of these techniques rather cumbersome for an inexperienced user. For these algorithms, problems of convergence may arise especially when strain softening of concrete in compression is taken into account, and they may become unstable near the state of pure compression or tension. There exist three different methods to generate plane interaction curves for cross-sections under biaxial bending: (1) interaction curves for a given bending moment ratio N–M–M, [5], (2) load contours for a given axial load (M–M) [7] and (3) generate triplets of stress resultants on the failure surface by extending an arbitrary oriented straight line [4,10,11]. The plane interaction curves generated by these methods are depicted in Fig. 1. However it is important to note that, although claimed, not all the methods found in the literature generate genuinely plane curves. For instance the method proposed in [7] fails in some circumstances to draw the moment capacity contour, under a fixed axial load, and in order to overcome some divergences, the axial load value is slightly adjusted.

In either technique, the elasto-plastic properties of the cross-section are modelled by explicit integration of stresses and strains over the cross-section area. Thus, a further complication is represented by the nonlinear constitutive law that is usually assumed for concrete in compression. Some existing methods for the analysis of cross-sections under axial load and biaxial bending rely on the numerical integration of stress resultants using the well known "fiber decomposition method" where the cross-section is decomposed into filaments and the section response is computed by composing the uniaxial behaviour of each filament [9]. These techniques are not numerically efficient, due to the large amount of information needed to characterize the section and the high number of operations required by stress integration with an allowable error level [9], but, on the other hand, they can employ various strain distributions, or stress–strain diagrams that can be used for cyclic loading. Rodriguez and Ochoa [5] presented a method to determine the biaxial interaction diagrams for any orientation of the neutral axis of RC short columns with any geometry, obtaining analytical closed form integral expressions of the internal forces. Sfakianakis [8] developed an alternative method, based on the fiber decomposition approach that employs computer graphics as a computational tool for the integration of normal stresses over the section area. Based on Green's theorem Rotter [3] and then Fafitis [6] developed numerical procedures for numerical integration of concrete in compression, but these formulations are limited to fully confined concrete (i.e. the descending curve of the concrete is not included) and to polygonal cross-sections only. Based on the secant [4,11] and tangent [10] stiffness strategy for the solution of nonlinear equilibrium equations, Rosati and co-workers developed several algorithms and boundary integration formulas for evaluating the ultimate strength capacity of polygonal and circular RC cross-sections. These algorithms are limited to fully confined concrete.

The main objective of this paper is to present a new formulation by which the biaxial interaction diagrams and moment capacity contours of a composite steel–concrete cross-section can be determined, which make use of an incremental-iterative procedure based on arc-length constraint equations.

The proposed procedure adopts a tangent stiffness strategy for the solution of the nonlinear equilibrium equations thus resulting in a high rate of convergence. Based on Green's theorem, the domain integrals appearing in the definition of stress resultants and tangent stiffnesses are evaluated in terms of boundary integrals when the section boundary is rectilinear or circular.

Considering the solution of nonlinear equilibrium equations, the proposed incremental-iterative method is advantageous with

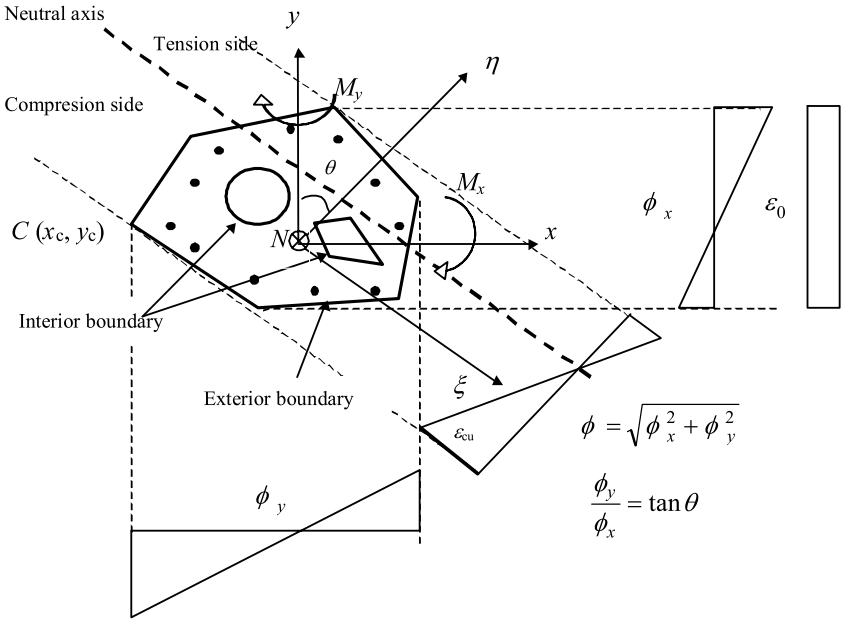

Fig. 2. Model of arbitrary composite cross-section.

respect to the existing ones [5,7,13], in that the solution is obtained by solving just two coupled nonlinear equations and the convergence stability is not sensitive to the initial/starting values of the basic variables (i.e. the ultimate curvatures about global axes ϕ_x and ϕ_y), involved in the iterative process. For all cases examined herein it has been found that starting the iterative process with the initial curvatures $\phi_x = 0$ and $\phi_y = 0$ the convergence is achieved in a low number of iterations.

Most of the existing methods that use iterative procedures [5,7] are not general, they can compute either interaction curves for a given bending moment ratio [5] or load contours for a given axial load [7]. As will be presented in the next sections, the proposed approach can handle both types of interaction curves. Besides, the proposed method can provide directly the ultimate resistance of the cross-section, supposing that one or two components of the section forces are known. This is a particularly important feature that can be used efficiently in the nonlinear structural analysis program, to detect directly whether the representative point of the cross-section lies on the yielding surfaces, without the need of knowing in advance the whole interaction diagram or moment capacity contour. For instance, for given bending moments (M_x, M_y) we can determine directly the axial force resistance N and also for given bending moment's ratio and axial force N, the ultimate values of the bending moments can be directly evaluated. However, when the axial force N and one of the bending moments, for instance M_x are given, the associated ultimate value of the bending moment M_y is not unique (see Fig. 5c), because at least two strain distributions fulfill this load constraint (see Eq. (6)). In this case the search direction to one of the possible solutions cannot be controlled. The linear constraint given by Eq. (6) is used, in the current paper, only for drawing the moment capacity contours.

Moreover using the proposed method we have found that near the axial load capacity under pure compression, when the strain softening of the concrete is taken into account, the solution is not unique which implies non-convexity of the failure surface in these situations. Therefore, the proposed approach based on the arc-length constraint strategy is essential to assure the convergence of the entire process and to determine all possible solutions.

2. Mathematical formulation

2.1. Assumptions and problem definition

Consider the cross-section subjected to the action of the external bending moments about both global axes and axial force as shown in Fig. 2. The cross-section may assume any shape with multiple polygonal or circular openings. However, the approach presented in this paper can handle only composite steel–concrete sections where the steel part is completely surrounded by concrete. It is assumed that the plane section remains plane after deformation. This implies a perfect bond between the steel and concrete components of a composite concrete–steel cross-section. Shear and torsional interaction and shrinkage effects are not accounted for in the concrete constitutive model. Thus the resultant strain distribution corresponding to the curvatures about global axes $\mathbf{\Phi} = \{\phi_x, \phi_y\}$ and the axial compressive strain ε_0 can be expressed at a generic point (x, y) in a linear form as:

$$\varepsilon = \varepsilon_0 + \phi_x y + \phi_y x. \tag{1}$$

The constitutive relation for concrete under compression is represented by a combination of a second-degree parabola and a straight line, Eq. (2), as depicted in Fig. 3:

$$f_c = \begin{cases} f_c'' \left(2\dfrac{\varepsilon}{\varepsilon_{c0}} - \dfrac{\varepsilon^2}{\varepsilon_{c0}^2} \right), & \varepsilon \le \varepsilon_0 \\ f_c'' \left(1 - \gamma \left(\dfrac{\varepsilon - \varepsilon_{c0}}{\varepsilon_{cu} - \varepsilon_{c0}} \right) \right), & \varepsilon > \varepsilon_0 \end{cases} \tag{2}$$

where γ represents the degree of confinement in the concrete and allows for the modelling of creep and confinement in concrete by simply varying the crushing strain ε_{c0} and γ, respectively. The tensile strength of concrete is neglected. Elastic–perfectly plastic stress–strain relationship, both in tension and in compression, is assumed for the structural steel and the steel reinforcing bars (Fig. 4). The strain hardening of steel is neglected.

The cross-section reaches its failure limit state when the strain in the extreme compression fiber of the concrete, or in the extreme tensioned steel fiber, attains the ultimate value. Consequently, at ultimate strength capacity the equilibrium is satisfied when the external forces are equal to the internal ones and in the most

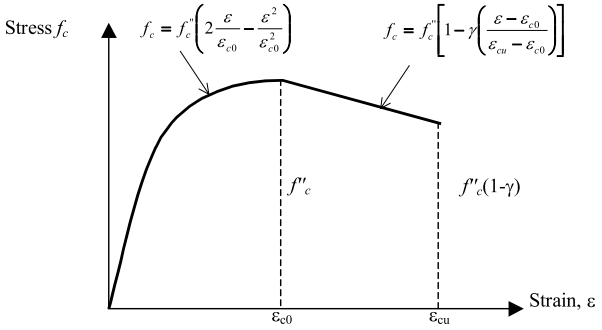

Fig. 3. Stress–strain relationships for concrete in compression.

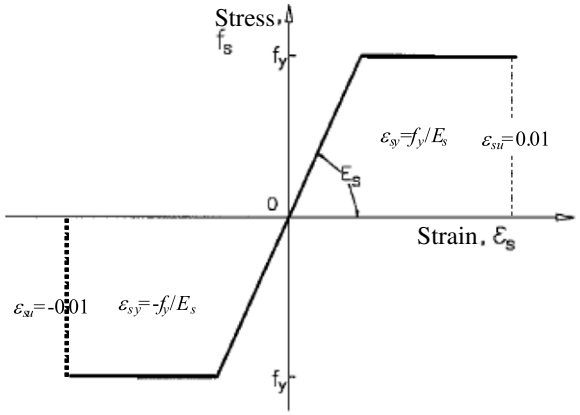

Fig. 4. Stress–strain relationships for steel.

compressed or tensioned point the ultimate strain is attained. These conditions can be represented mathematically in terms of the following nonlinear system of equations as:

$$\begin{cases} \int_A \sigma(\varepsilon(\varepsilon_0, \phi_x, \phi_y))\mathrm{d}A - N = 0 \\ \int_A \sigma(\varepsilon(\varepsilon_0, \phi_x, \phi_y))y\mathrm{d}A - M_x = 0 \\ \int_A \sigma(\varepsilon(\varepsilon_0, \phi_x, \phi_y))x\mathrm{d}A - M_y = 0 \\ \varepsilon_0 + \phi_x y_c(\phi_x, \phi_y) + \phi_y x_c(\phi_x, \phi_y) - \varepsilon_u = 0 \end{cases} \tag{3}$$

in which N, M_x, M_y, $\varepsilon_0, \phi_x, \phi_y$ represent the unknowns. In Eqs. (3) the first three relations represent the basic equations of equilibrium for the axial load N and the biaxial bending moments M_x, M_y, respectively, given in terms of the stress resultants. The last equation represents the ultimate strength capacity condition, that is, in the most compressed or the most tensioned point the ultimate strain is attained; in this equation $x_c(\phi_x, \phi_y)$ and $y_c(\phi_x, \phi_y)$ represent the coordinates of the point in which this condition is imposed. The coordinates of the "constrained" point can be always determined for each inclination of the neutral axis defined by the parameters ϕ_x and ϕ_y, and ε_u represents the ultimate strain either in the most compressed concrete point or in the most tensioned reinforcement steel fiber. The stresses in Eqs. (3) are calculated using the fiber strains and the constitutive relations. Obviously the system given by Eqs. (3) is an undetermined nonlinear system of equations (i.e. it has more unknowns than equations) and it has, in general, infinite many solutions. However the system has the "forces" unknowns decoupled and using strain distributions corresponding to a failure condition it is possible to calculate, point by point, the entire failure surface, by varying the position and the inclination of the neutral axis through the parameters $\varepsilon_0, \phi_x, \phi_y$ and computing the ultimate resistances N, M_x, M_y of the cross-section through Eq. (3). Although in this way we can compute the failure surface, the resulting interaction diagrams, being three dimensional, are difficult to plot and have limited practical applicability. In practice, instead, it is often desirable to have plane interaction diagrams that are easier to use and interpret.

Under the above assumptions, the problem of the ultimate strength analysis of composite (concrete–steel) cross-sections can be formulated as:

Given a strain distribution corresponding to a failure condition (i.e. maximum strains attained either at the outer compressed point of the concrete or in the most tensioned reinforcement steel fiber), find the ultimate resistances N, M_x, M_y so as to fulfill the basic equations of equilibrium and one of the following linear constraints:

$$\begin{cases} L_1(N, M_x, M_y) \equiv M_x - M_{x0} = 0 \\ L_2(N, M_x, M_y) \equiv M_y - M_{y0} = 0 \end{cases} \tag{4}$$

$$\begin{cases} L_1(N, M_x, M_y) \equiv N - N_0 = 0 \\ L_2(N, M_x, M_y) \equiv M_y - \tan(\alpha)M_x = 0 \end{cases} \tag{5}$$

$$\begin{cases} L_1(N, M_x, M_y) \equiv N - N_0 = 0 \\ L_2(N, M_x, M_y) \equiv M_x - M_{x0} = 0 \end{cases} \tag{6}$$

where N_0, M_{x0}, M_{y0} represent the given axial force and bending moments, respectively, and α represents the angle formed by the bending moments M_x and M_y measured form the positive direction of the x axis.

A solution of the problem stated above is searched for iteratively as will be presented in the next sections of the paper. As can be seen in Fig. 5, at least two strain distributions fulfill the load constraints (4) and (6). As will be detailed in the next sections, when constraints (4) are considered, the search direction can be controlled by starting the iterative process either with a strain distribution associated with failure of the cross-section in compression (i.e. solution 1 in Fig. 5a) or with a strain distribution associated with failure of the cross-section in tension (i.e solution 2 in Fig. 5a). When the constraints (6) are considered the search direction cannot be controlled. However, using the constraints (5) for a given value of the angle α, measured from the positive direction of the x axis, the solutions can be detected, solution 1 for angle (α) and solution 2 for angle ($\alpha + \pi$), respectively (Fig. 5b).

The general solution procedure is based on the solution of nonlinear system (3) for one of the three linear constraints defined by Eqs. (4)–(6). Corresponding to each linear constraints we can define a point on the failure surface as: (I) when constraints (4) are injected in nonlinear system (3), a point on the failure surface is defined by computing the axial resistance N associated with a failure criterion and for a fixed value of bending moments (M_x, M_y); (II) when constraints (5) are used, the point on the failure surface is defined for a fixed axial load (N) and a given bending moment's ratio; (III) when constraints (6) are used, the point is associated with a fixed axial load (N) and a given bending moment M_x about x axis. This is then used as the basis for one of the two analysis options: (1) a plot of the vertical sections of the failure surface that are typically called interaction diagrams, (2) a plot of the horizontal sections of the failure surface that are typically called moment capacity contours or loading contours. These diagrams are obtained by incrementally varying the fixed generalized force values and solving for corresponding variable force and ultimate curvatures. All these situations are graphically illustrated in Fig. 5. It is important to note that, although the paper mainly concerns the drawing of the yielding diagrams, the proposed method, can be applied to provide directly the ultimate resistances of the cross-section, in the hypothesis that one or two

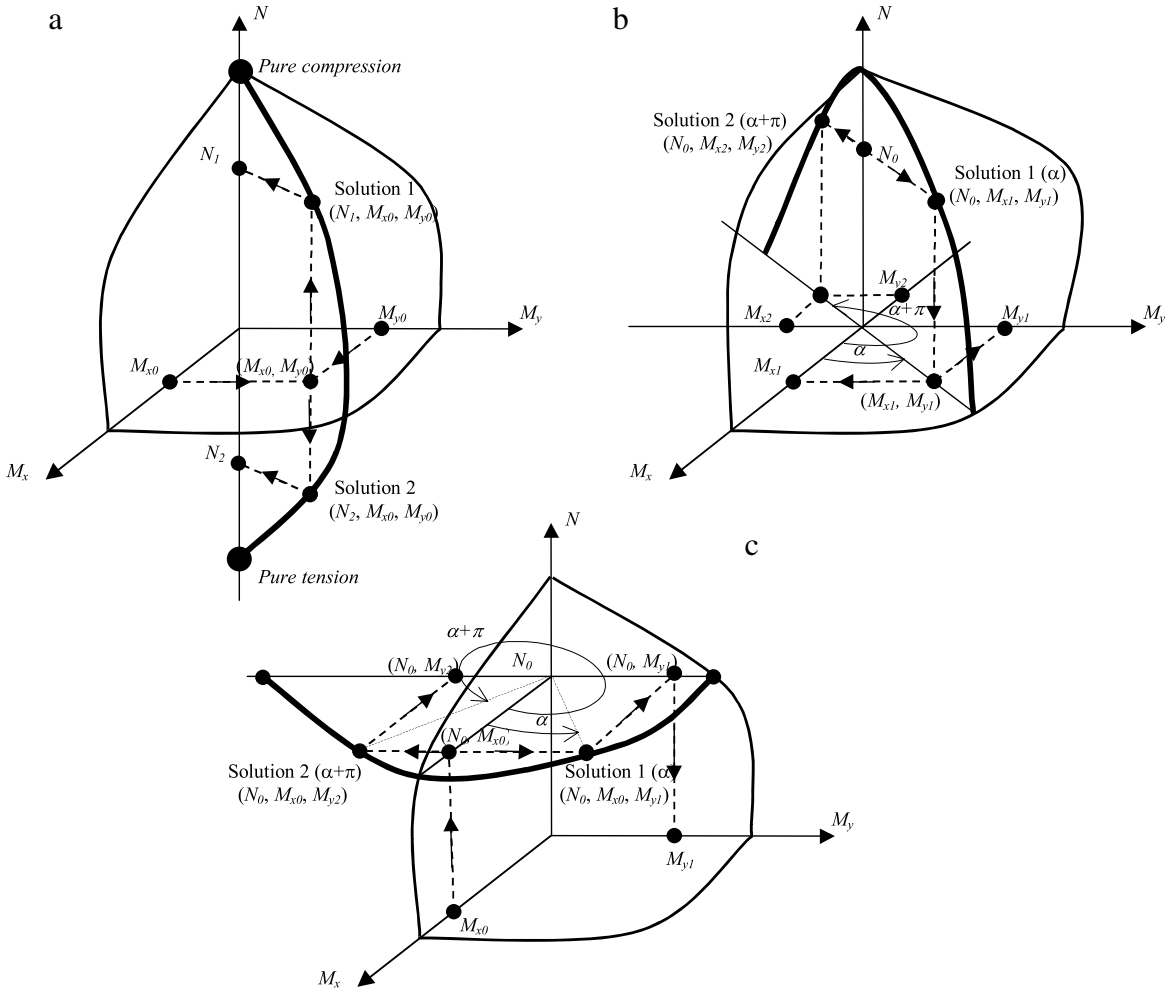

Fig. 5. Solution procedures. (a) Interaction diagrams for given bending moments; (b) Interaction diagrams for given axial load and bending moment's ratio; (c) Moment capacity contours for given axial force and bending moment M_x.

components of the section forces are known. This is a particularly important feature of the proposed method that can be used efficiently in the nonlinear structural analysis program, to detect whether a load value lies or not on the yielding surface, without the need of knowing in advance the whole interaction diagram or moment capacity contour. This feature will be illustrated in the Computational examples section.

2.2. Method of solution

An incremental-iterative procedure based on arc-length constraint equation is proposed in order to determine the biaxial strength of an arbitrary composite steel–concrete cross-section according to the already described situations. The failure diagrams correspond either to maximum strains attained at the outer compressed point of the concrete section (i.e. ε_u equal to the compressive strain at failure) or to maximum strains attained in the most tensioned reinforcement steel fiber (i.e. ε_u equal to the tensile steel strain at failure). Consider an irregular composite section as shown in Fig. 2. The global x, y axes of the cross-section could have their origin either in the elastic or plastic centroid of the cross-section. For each inclination of the neutral axis defined by the parameters ϕ_x and ϕ_y the farthest point on the compression side (or the most tensioned steel bar position) is determined (i.e. the point with coordinates x_c, y_c). We assume that at this point the failure condition is met:

$$\varepsilon_0 + \phi_x y_c + \phi_y x_c = \varepsilon_u. \tag{7}$$

Hence, the axial strain ε_0 can be expressed as:

$$\varepsilon_0 = \varepsilon_u - (\phi_x y_c + \phi_y x_c). \tag{8}$$

Taking into account equation (1), the resulting strain distribution corresponding to the curvatures ϕ_x and ϕ_y can be expressed in linear form as:

$$\varepsilon(\phi_x, \phi_y) = \varepsilon_u + \phi_x(y - y_c) + \phi_y(x - x_c). \tag{9}$$

In this way, substituting the strain distribution given by Eq. (9) in the basic equations of equilibrium, the unknown ε_0 together with the failure constraint equation can be eliminated from nonlinear system (3). Thus, the basic equations of equilibrium together with the linear constraints equations (4)–(6) form a determined nonlinear system of equations (i.e. 5 equations and 5 unknowns):

$$\begin{cases} \int_A \sigma(\varepsilon(\phi_x, \phi_y))\mathrm{d}A - N = 0 \\ \int_A \sigma(\varepsilon(\phi_x, \phi_y))y\mathrm{d}A - M_x = 0 \\ \int_A \sigma(\varepsilon(\phi_x, \phi_y))x\mathrm{d}A - M_y = 0 \\ L_1(N, M_x, M_y) = 0 \\ L_2(N, M_x, M_y) = 0 \end{cases} \tag{10}$$

and the solutions can be obtained iteratively following an approach outlined in the next sections. It is important to note that the

curvatures ϕ_x and ϕ_y, solutions of the above system of equations, are associated with a failure criterion and represent the ultimate sectional curvatures.

2.2.1. Interaction diagrams for given bending moments

In this case introducing constraints (4) in system (10) the problem of the ultimate strength analysis of cross-section can be expressed as:

$$\begin{cases} \int_A \sigma(\varepsilon(\phi_x, \phi_y))\mathrm{d}A - N = 0 \\ \int_A \sigma(\varepsilon(\phi_x, \phi_y))y\mathrm{d}A - M_{x0} = 0 \\ \int_A \sigma(\varepsilon(\phi_x, \phi_y))x\mathrm{d}A - M_{y0} = 0 \end{cases} \tag{11}$$

in which axial load N and curvatures ϕ_x and ϕ_y represent the unknowns. If we regard the curvatures ϕ_x and ϕ_y as independent variables in the axial force equation, then

$$N = \int_A \sigma(\varepsilon(\phi_x, \phi_y))\mathrm{d}A \tag{12}$$

and the curvatures ϕ_x and ϕ_y are obtained by solving the following nonlinear system of equations:

$$\begin{cases} \int_A \sigma(\varepsilon(\phi_x, \phi_y))y\mathrm{d}A - M_{x0} = 0 \\ \int_A \sigma(\varepsilon(\phi_x, \phi_y))x\mathrm{d}A - M_{y0} = 0. \end{cases} \tag{13}$$

The above system can be solved numerically using, for instance, the load-controlled Newton method and taking into account the fact that the stresses are implicit functions of curvatures through the resultant strain distribution given by Eq. (9). In this way, for given bending moments we can obtain directly the axial force resistance N and a point on the failure surface associated with the known bending moments. As already mentioned, at least two strain distributions fulfill Eq. (13) (see Fig. 5a). However, the search direction can be controlled so as to enforce the iterative process to converge to one of them. For instance, starting the iterative process enforcing the failure of the cross-section in compression (i.e. in Eq. (9) ε_u represents the compressive strain at failure and x_c and y_c represent the coordinates of the most compressed point) the solution 1 will be obtained (Fig. 5a). On the other hand, enforcing the failure of the cross-section in tension, the solution 2 (Fig. 5a) will be attained.

The iterative procedure starts specifying the bending moments M_{x0} and M_{y0}. At the very first iteration, starting with the initial curvatures $\phi_x = 0$ and $\phi_y = 0$ the tangent stiffness matrix $\mathbf{K}_T$ (see Eq. (20)) could become singular, because in this case the strain profile over the cross-section is uniform with maximum ultimate strain in compression or tension, which implies zero tangent modulus of elasticity. In this case one can simply start the iteration process with the secant modulus of elasticity in the evaluation of the tangent stiffness coefficients of the cross-section. For the next iterations an adaptive-descent algorithm [14] is applied in order to avoid the convergence difficulties related to the negative definition of the tangent stiffness matrix that can occur during the iterative process. Adaptive descent is a technique which switches to a secant matrix if convergence difficulties are encountered, and switches back to the full tangent as the solution convergences, resulting in the desired rapid convergence rate. If the bending moments M_{x0} and M_{y0} are outside the moment capacity contour, this means that for any axial load the applied load combination (M_{x0}, M_{y0}) exceeds the ultimate state condition of the cross-section and divergence of the iterative process will be signalled.

This formulation can be generalized for the construction of the entire interaction diagram at given bending moments. In this respect, the bending moments can be parametrized by a single variable λ, the load parameter, defining the intensity of the bending moments, and system (13) can be rewritten as:

$$\begin{cases} \int_A \sigma(\varepsilon(\phi_x, \phi_y))y\mathrm{d}A - \lambda M_{x0} = 0 \\ \int_A \sigma(\varepsilon(\phi_x, \phi_y))x\mathrm{d}A - \lambda M_{y0} = 0 \end{cases} \tag{14}$$

where the curvatures ϕ_x and ϕ_y and the load amplifier factor λ represent the unknowns.

This can be rewritten in terms of nonlinear system of equations in the following general form:

$$\mathbf{F}(\lambda, \mathbf{\Phi}) = \mathbf{f}^{\mathrm{int}} - \lambda \mathbf{f}^{\mathrm{ext}} = \mathbf{0} \tag{15}$$

where $\mathbf{f}^{\mathrm{ext}} = \begin{bmatrix} M_{x0} & M_{y0} \end{bmatrix}^T$ is the reference load vector (reference bending moments),

$$\mathbf{f}^{\mathrm{int}} = \left[M_x^{\mathrm{int}} = \int_A \sigma(\varepsilon(\phi_x, \phi_y))y\mathrm{d}A \quad M_y^{\mathrm{int}} = \int_A \sigma(\varepsilon(\phi_x, \phi_y))x\mathrm{d}A \right]^T$$

is the internal bending moments vector, computed as functions of the curvatures $\mathbf{\Phi} = [\phi_x\ \phi_y]^T$. To obtain the equilibrium path, a proper parametrization is needed. A common setting of a continuation process is to augment the equilibrium equations (15) with a constraint [15]. In this case the curvature–moment constraint can be defined in the following form:

$$\mathbf{H}(\lambda, \mathbf{\Phi}) = \begin{cases} \mathbf{f}^{\mathrm{int}} - \lambda \mathbf{f}^{\mathrm{ext}} = \mathbf{0} \\ g(\lambda, \mathbf{\Phi}) = 0 \end{cases} \tag{16}$$

where $g(\lambda, \mathbf{\Phi})$ is a constraint equation [15].

In this procedure, commonly called arc-length method, these equations are solved in a series of steps or increments, usually starting from the unloaded state ($\lambda = 0$), and the solution of Eq. (16), referred to as equilibrium path, is obtained by solving directly the equilibrium equations together with the auxiliary constraint equation, making a total of three simultaneous equations. Alternatively, instead of solving Eq. (16) directly, an indirect solution scheme for the constraint equation may be introduced for solving Eq. (16) [15]. The load increment is governed by the following constraint equation having the general form:

$$\Delta\mathbf{\Phi}^T \Delta\mathbf{\Phi} + \Delta\lambda^2 \Psi^2 \mathbf{f}^{\mathrm{ext}T} \mathbf{f}^{\mathrm{ext}} - \Delta l^2 = 0 \tag{17}$$

where $\mathbf{\Delta\Phi}$ is the vector of curvatures, $\Delta\lambda$ is the incremental load factor, Δl is the specified arc length for the current increment and Ψ is the scaling parameter for loading and curvature terms. According to the indirect arc-length technique, the iterative changes of curvature vector $\delta\mathbf{\Phi}$ for the new unknown load level $\Delta\lambda_{k+1} = \Delta\lambda_k + \delta\lambda$, is written as:

$$\delta\mathbf{\Phi} = -\mathbf{K}_T^{-1}\mathbf{F} + \delta\lambda \mathbf{K}_T^{-1}\mathbf{f}^{\mathrm{ext}} = \delta\mathbf{F} + \delta\lambda\delta\mathbf{\Phi}_T \tag{18}$$

where $\mathbf{F}$ represents the out-of-balance force vector (Eq. (15)) and $\mathbf{K}_T$ represents the tangent stiffness matrix of the cross-section:

$$\mathbf{K}_T = \left(\frac{\partial \mathbf{F}}{\partial \mathbf{\Phi}} \right) = \begin{bmatrix} \dfrac{\partial M_x^{\mathrm{int}}}{\partial \phi_x} & \dfrac{\partial M_x^{\mathrm{int}}}{\partial \phi_y} \\ \dfrac{\partial M_y^{\mathrm{int}}}{\partial \phi_x} & \dfrac{\partial M_y^{\mathrm{int}}}{\partial \phi_x} \end{bmatrix} \tag{19}$$

in which the partial derivatives are expressed with respect to the strains and stresses evaluated at current iteration k. Assuming the

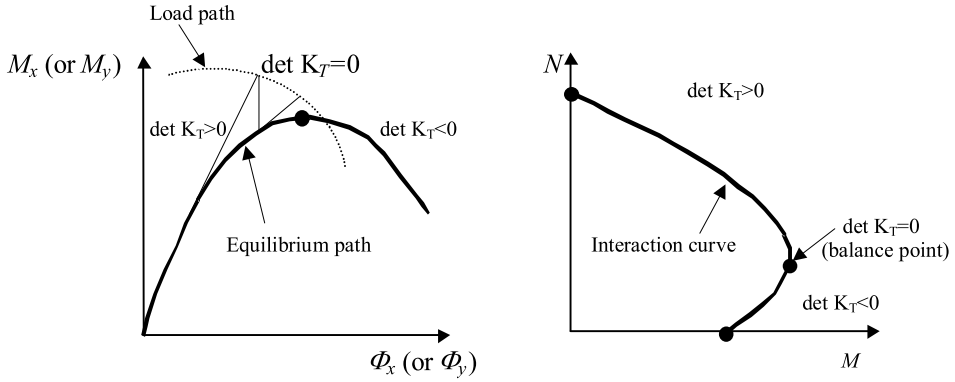

Fig. 6. Geometrical representation of the proposed method.

strain distribution given by Eq. (9), the coefficients of the stiffness matrix can be symbolically evaluated as:

$$\begin{aligned}
k_{11} &= \frac{\partial M_x^{\text{int}}}{\partial \phi_x} = \frac{\partial}{\partial \phi_x}\int_A \sigma(\varepsilon(\phi_x,\phi_y))y\mathrm{d}A \\
&= \int_A \frac{\partial \sigma}{\partial \varepsilon}\frac{\partial \varepsilon}{\partial \phi_x}y\mathrm{d}A = \int_A E_T y(y-y_c)\mathrm{d}A \\
k_{12} &= \frac{\partial M_x^{\text{int}}}{\partial \phi_y} = \frac{\partial}{\partial \phi_y}\int_A \sigma(\varepsilon(\phi_x,\phi_y))y\mathrm{d}A \\
&= \int_A \frac{\partial \sigma}{\partial \varepsilon}\frac{\partial \varepsilon}{\partial \phi_y}y\mathrm{d}A = \int_A E_T y(x-x_c)\mathrm{d}A \\
k_{21} &= \frac{\partial M_y^{\text{int}}}{\partial \phi_x} = \frac{\partial}{\partial \phi_x}\int_A \sigma(\varepsilon(\phi_x,\phi_y))x\mathrm{d}A \\
&= \int_A \frac{\partial \sigma}{\partial \varepsilon}\frac{\partial \varepsilon}{\partial \phi_x}x\mathrm{d}A = \int_A E_T x(y-y_c)\mathrm{d}A \\
k_{22} &= \frac{\partial M_y^{\text{int}}}{\partial \phi_y} = \frac{\partial}{\partial \phi_y}\int_A \sigma(\varepsilon(\phi_x,\phi_y))x\mathrm{d}A \\
&= \int_A \frac{\partial \sigma}{\partial \varepsilon}\frac{\partial \varepsilon}{\partial \phi_y}x\mathrm{d}A = \int_A E_T x(x-x_c)\mathrm{d}A
\end{aligned} \tag{20}$$

where the coefficients k_{ij} are expressed in terms of the tangent modulus of elasticity E_t and the coordinates x_c, y_c of the "constrained" point. As can be seen in Eq. (9) the strain distribution is explicitly determined by the coordinates x_c, y_c of the "constrained" point. During the iterative process, these coordinates are assumed to be known from the previous iteration (i.e. from the previous values of curvatures ϕ_x and ϕ_y) and, consequently, can be assumed as constants in the evaluation of the above stiffness matrix coefficients. Hence, at current iteration, the partial derivatives of the coordinates x_c and y_c upon ϕ_x and ϕ_y, being zero, are not included in the expression of k_{ij} in Eqs. (20). Thus the incremental curvatures for the next iteration can be written as:

$$\Delta\boldsymbol{\Phi}_{k+1} = \Delta\boldsymbol{\Phi}_k + \delta\boldsymbol{\Phi}. \tag{21}$$

Substituting the incremental curvatures in the constraint equation (17) yields the expression for the required correction of the incremental load factor:

$$a_1\delta\lambda^2 + a_2\delta\lambda + a_3 = 0 \tag{22}$$

where

$$\begin{aligned}
a_1 &= \delta\boldsymbol{\Phi}_T^T\delta\boldsymbol{\Phi}_T + \psi^2\mathbf{f}^{\text{ext}T}\mathbf{f}^{\text{ext}} \\
a_2 &= 2\delta\boldsymbol{\Phi}_T(\Delta\boldsymbol{\Phi}+\delta\mathbf{F}) + 2\Delta\lambda\psi^2\mathbf{f}^{\text{ext}T}\mathbf{f}^{\text{ext}} \\
a_3 &= (\Delta\boldsymbol{\Phi}+\delta\mathbf{F})^T(\Delta\boldsymbol{\Phi}+\delta\mathbf{F}) - \Delta l^2 + \Delta\lambda^2\psi^2\mathbf{f}^{\text{ext}T}\mathbf{f}^{\text{ext}}.
\end{aligned} \tag{23}$$

These coefficients can be computed from the results of the kth iteration, so that the quadratic equation can be solved and a root can be chosen for $\delta\lambda$. Then Eq. (18) is used to compute the next trial curvature increments $\Delta\boldsymbol{\Phi}_{k+1}$. This procedure is iterated until convergence with respect to a suitable norm is attained. Assuming that a point $({}^{\tau}\boldsymbol{\Phi}, {}^{\tau}\lambda)$ of the equilibrium path has been reached, the next point $({}^{\tau+\Delta\tau}\boldsymbol{\Phi}, {}^{\tau+\Delta\tau}\lambda)$ of the equilibrium path is then computed by updating the loading factor and curvatures as:

$$\begin{aligned}
{}^{\tau+\Delta\tau}\lambda &= {}^{\tau}\lambda + \Delta\lambda_{k+1} \\
{}^{\tau+\Delta\tau}\boldsymbol{\Phi} &= {}^{\tau}\boldsymbol{\Phi} + \Delta\boldsymbol{\Phi}_{k+1}.
\end{aligned} \tag{24}$$

In this way, with curvatures and loading factor known, the axial force resistance N is computed on the basis of the resultant strain distribution corresponding to the curvatures ϕ_x and ϕ_y through Eq. (12), and the ultimate bending moments, M_x and M_y, are obtained by scaling the reference external moments M_{x0} and M_{y0} through the current loading factor λ given by Eqs. (24). The scaling parameter Ψ has a little influence in the results and has been taken as zero in the current approach. As a result, constraint (17) should be considered "cylindrical" rather than "spherical" [15].

In this way, adopting an automatic step length adaptation scheme for the loading factor, the entire interaction diagram of the cross-section can be constructed at given bending moments. Graphical representation of the present method according to Eq. (16) is depicted in Fig. 6. It is important to note that the stiffness matrix of cross-section K_T, given by Eq. (20), could become negative definite during the iterative process (see Fig. 6), and therefore the above procedure based on the arc-length constraint equation is essential to overcome these difficulties. When the tangent stiffness matrix of the section is singular (i.e. at the very first iteration of the algorithm), secant stiffness matrix is adopted.

Fig. 7 shows a simplified flowchart of this analysis algorithm, whereas some computational aspects are briefly described next.

The incremental-iterative procedure starts specifying the fixed bending moments M_{x0} and M_{y0}, the initial load increment $\Delta\lambda_0$ and initial arc-length increment Δl_0. Small bending moments (i.e near zero) and small initial increment ($\Delta\lambda_0 = 0.01$) represent suitable starting values. However, the user will have little idea of an appropriate magnitude for a starting length increment Δl_0. Two solutions have been implemented. The first is to apply a preliminary load-controlled step, as described previously (see Eq. (13)), and, from the output, a suitable starting value can be estimated. Alternatively, the user may start by specifying a load increment $\Delta\lambda_0$. The incremental curvature vector, $\Delta\boldsymbol{\Phi}$, can then be computed from:

$$\Delta\boldsymbol{\Phi} = \Delta\lambda_0\mathbf{K}_T^{-1}\mathbf{f}^{\text{ext}} \tag{25}$$

and, a starting length increment, Δl_0, can be obtained as:

$$\Delta l_0 = \Delta\lambda_0\sqrt{\Delta\boldsymbol{\Phi}^T\Delta\boldsymbol{\Phi}}. \tag{26}$$

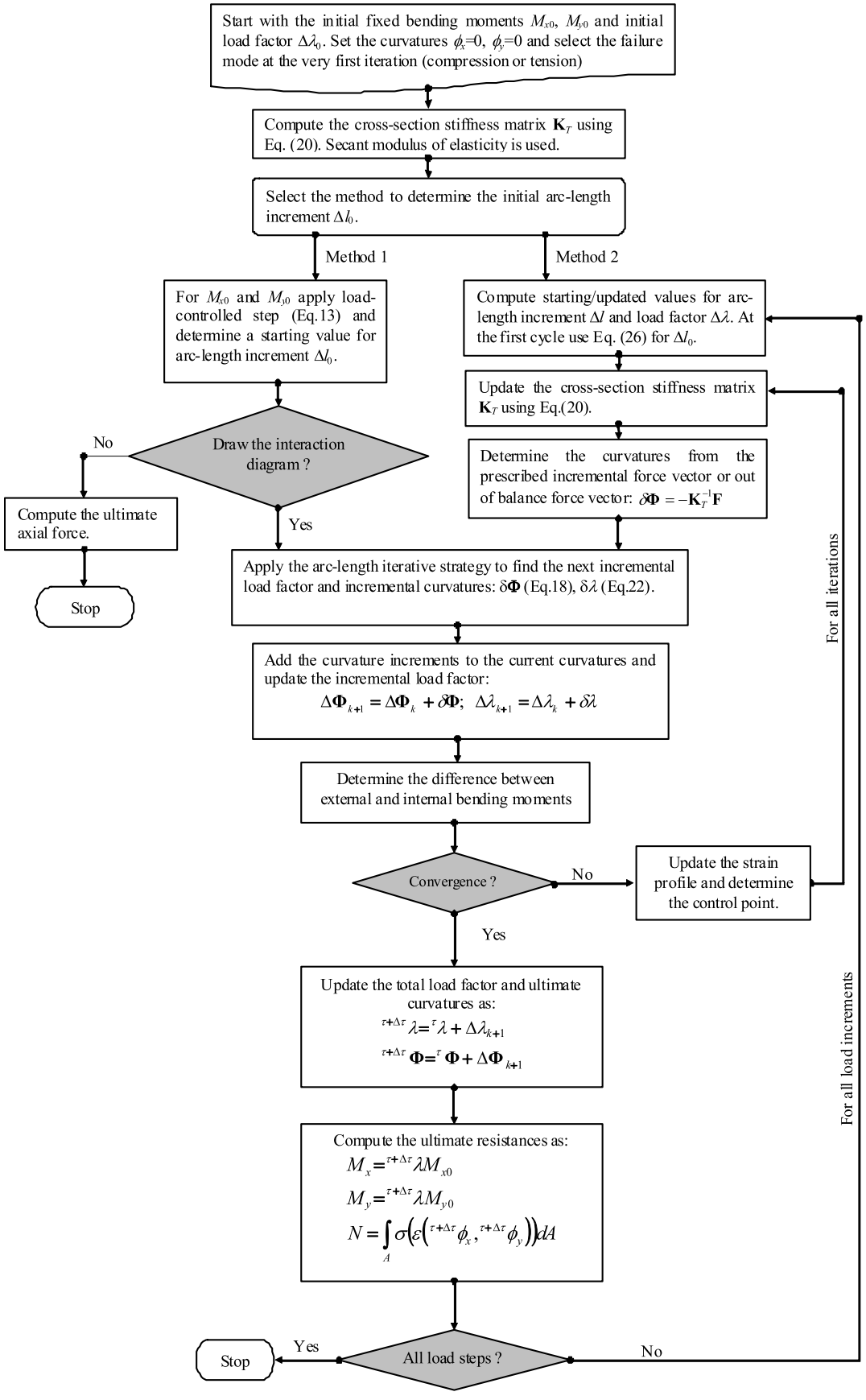

Fig. 7. Interaction diagrams for given bending moments. Analysis flowchart.

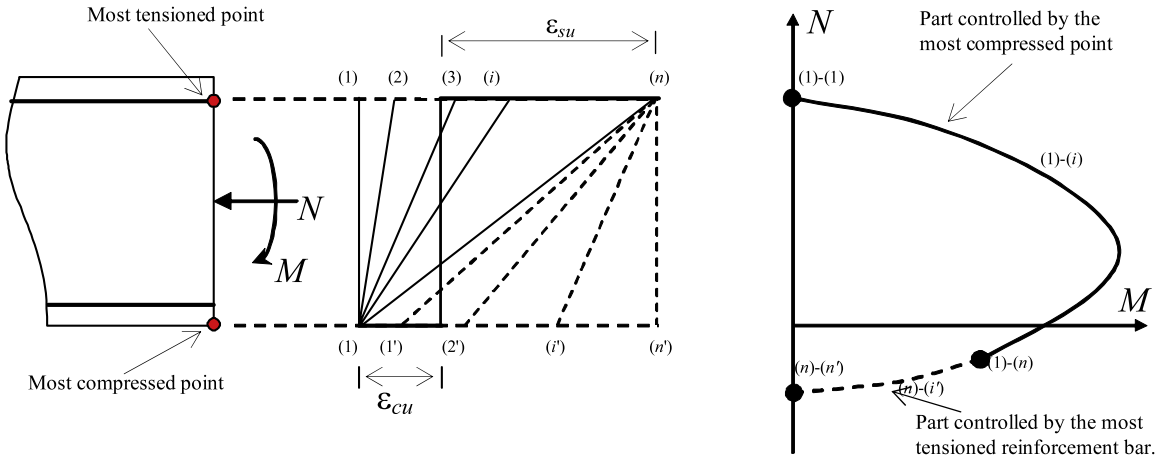

Fig. 8. Strain profiles at failure and the associated interaction diagram.

The incremental-iterative procedure is completely adaptive: it starts with the initial load factor and the step size is scaled by the convergence speed, relating the number of iterations used in the previous step to a desired value. The adjustment used by Ramm [16] is adopted. This technique leads to the provision of suitable magnitude of increments, as a function of the degree of nonlinearity: small increments when the response is most "nonlinear" and large increments when the response is most "linear".

The convergence criterion is expressed as a ratio of the norm of the out-of-balance force vector to the norm of the total applied load in each incrementation. So the solution is assumed to have converged if:

$$\frac{\sqrt{\mathbf{F}^T\mathbf{F}}}{{}^{\tau+\Delta\tau}\lambda\sqrt{\mathbf{f}^{\mathrm{ext}T}\mathbf{f}^{\mathrm{ext}}}} \le TOL \tag{27}$$

where ${}^{\tau+\Delta\tau}\lambda$ represents the current load factor and *TOL* is the specified computational tolerance, usually taken as 1E−5.

As was stated previously, the failure of the cross-section can be controlled either by the most compressed concrete point with $\varepsilon_u = \varepsilon_c$ or the most tensioned steel reinforcement bar with $\varepsilon_u = \varepsilon_s$. Starting the iterative process with control in compression, the interaction diagram will be evaluated from the compression side towards tension side, whereas enforcing the failure of the cross-section in tension, at the very first iteration, the interaction diagram is evaluated from the tension to compression side. During the iterative process these controlled points are automatically interchanged. For instance, assuming that the current iterations are conducted with the most compressed point (Fig. 8) the strain profiles are defined by the same ultimate compressive strain and by different strains at the level of the most tensioned point. After the strains in the most tensioned point equal or exceed the tensile steel strain at failure, the control point becomes the most tensioned point, and the process continues similarly, but with the coordinates of this point and associated ultimate steel strain. Fig. 8 presents different types of strain profiles during this process, defined by either the ultimate compressive strain (1, 2, . . .) or by the ultimate steel strain (1′, 2′, . . .).

When solving quadratic equation (22), to avoid the complex roots that sometimes may occur, the procedure proposed in [17] is used. Another issue concerning the applicability of the arc-length technique consists in the correct choice of the root during the iterative process, preventing divergence or the equilibrium path from doubling back on itself. Multiple rules can be found in the literature concerning root selection [18]. Minimum angle criterion or minimum residual norm proposed in [15] can be used at regular points of the solution path, but in some cases, for a very sharp "snap-back" both methods fail to assure convergence. On the other hand, the following simple criterion, that maximizes the incremental loading factor as a function of the sign of the tangent stiffness matrix determinant, has been found to be very efficient for all cases examined herein. Hence, the root in Eq. (22) is selected according to:

$$\delta\lambda = \begin{cases} \delta\lambda_1, & t\delta\lambda_1 > t\delta\lambda_2 \\ \delta\lambda_2, & t\delta\lambda_1 \le t\delta\lambda_2 \end{cases} \tag{28}$$

in which t represents the sign of the stiffness matrix determinant:

$$t = \mathrm{sign}(\det \mathbf{K}_T). \tag{29}$$

This criterion is very simple to be implemented, prevents the numerical difficulties associated with divergence and avoids the possibility that the equilibrium path doubles back on itself.

2.2.2. Interaction diagrams for given axial load N and bending moment's ratio

With linear constraints (5), nonlinear system (10) becomes:

$$\begin{cases} \displaystyle\int_A \sigma(\varepsilon(\phi_x,\phi_y))\mathrm{d}A - N_0 = 0 \\ \displaystyle\int_A \sigma(\varepsilon(\phi_x,\phi_y))x\mathrm{d}A - \tan\alpha\int_A \sigma(\varepsilon(\phi_x,\phi_y))y\mathrm{d}A = 0 \\ \displaystyle\int_A \sigma(\varepsilon(\phi_x,\phi_y))y\mathrm{d}A - M_x = 0 \end{cases} \tag{30}$$

in which the bending moment M_x and curvatures ϕ_x and ϕ_y represent the unknowns. Regarding the curvatures ϕ_x and ϕ_y as independent variables in the bending moment equation,

$$M_x = \int_A \sigma(\varepsilon(\phi_x,\phi_y))y\mathrm{d}A \tag{31}$$

and the curvatures ϕ_x and ϕ_y are determined by solving the following nonlinear system of equations:

$$\begin{cases} f_1(\phi_x,\phi_y) = \displaystyle\int_A \sigma(\varepsilon(\phi_x,\phi_y))\mathrm{d}A - N_0 = 0 \\ f_2(\phi_x,\phi_y) = \displaystyle\int_A \sigma(\varepsilon(\phi_x,\phi_y))x\mathrm{d}A \\ \quad -\tan\alpha\displaystyle\int_A \sigma(\varepsilon(\phi_x,\phi_y))y\mathrm{d}A = 0. \end{cases} \tag{32}$$

Hence, for a given value of axial force N_0 and a given bending moment ratio $\tan(\alpha) = M_y/M_x$, one may solve for ϕ_x and ϕ_y nonlinear system (30) and then determine the bending moment M_x using Eq. (31) and $M_y = \tan(\alpha)M_x$. The iterative procedure

starts with curvatures $\phi_x = 0$ and $\phi_y = 0$, specifying the axial force N_0 and the angle α, formed by the bending moments M_x and M_y measured from the positive direction of the x axis (see Fig. 5b). For the next iterations an adaptive-descent algorithm is applied. In this way, for a given value of axial force N_0 and a given bending moment ratio $\tan(\alpha) = M_y/M_x$ the ultimate strength capacity of the cross-section can be directly determined.

As in the previous case, described in Section 2.2.1, parametrizing the external axial force N_0 in Eq. (32) through a load parameter λ, system (32) can be rewritten in terms of nonlinear system of equations in the following general form

$$\mathbf{F}(\lambda, \mathbf{\Phi}) = \mathbf{f}^{\text{int}} - \lambda \mathbf{f}^{ext} = \mathbf{0} \tag{33}$$

where

$$\mathbf{f}^{\text{ext}} = \begin{bmatrix} N_0 & 0 \end{bmatrix}^T \tag{34}$$

$$\mathbf{f}^{\text{int}} = \begin{bmatrix} \int_A \sigma(\varepsilon(\phi_x, \phi_y))\mathrm{d}A & \int_A \sigma(\varepsilon(\phi_x, \phi_y))x\mathrm{d}A \\ & -\tan\alpha \int_A \sigma(\varepsilon(\phi_x, \phi_y))y\mathrm{d}A \end{bmatrix}^T. \tag{35}$$

Following the arc-length technique, the interaction diagram can be determined, but in this case the iteration procedure is conducted with the tangent stiffness matrix computed as

$$\mathbf{K}_T = \begin{bmatrix} \dfrac{\partial f_1}{\partial \phi_x} & \dfrac{\partial f_1}{\partial \phi_y} \\ \dfrac{\partial f_2}{\partial \phi_x} & \dfrac{\partial f_2}{\partial \phi_x} \end{bmatrix} = \begin{bmatrix} k_{11} & k_{12} \\ k_{21} & k_{22} \end{bmatrix} \tag{36}$$

where the stiffness matrix coefficients are:

$$\begin{aligned}
k_{11} &= \frac{\partial f_1}{\partial \phi_x} = \frac{\partial}{\partial \phi_x}\int_A \sigma(\varepsilon(\phi_x, \phi_y))\mathrm{d}A \\
&= \int_A \frac{\partial \sigma}{\partial \varepsilon}\frac{\partial \varepsilon}{\partial \phi_x}\mathrm{d}A = \int_A E_T(y - y_c)\mathrm{d}A \\
k_{12} &= \frac{\partial f_1}{\partial \phi_y} = \frac{\partial}{\partial \phi_y}\int_A \sigma(\varepsilon(\phi_x, \phi_y))\mathrm{d}A \\
&= \int_A \frac{\partial \sigma}{\partial \varepsilon}\frac{\partial \varepsilon}{\partial \phi_y}\mathrm{d}A = \int_A E_T(x - x_c)\mathrm{d}A \\
k_{21} &= \frac{\partial f_2}{\partial \phi_x} = \frac{\partial}{\partial \phi_x}\left[\int_A \sigma(\varepsilon(\phi_x, \phi_y))x\mathrm{d}A \right. \\
&\quad \left. -\tan\alpha \int_A \sigma(\varepsilon(\phi_x, \phi_y))y\mathrm{d}A\right] \\
&= \int_A \frac{\partial \sigma}{\partial \varepsilon}\frac{\partial \varepsilon}{\partial \phi_x}x\mathrm{d}A - \tan(\alpha)\int_A \frac{\partial \sigma}{\partial \varepsilon}\frac{\partial \varepsilon}{\partial \phi_x}y\mathrm{d}A \\
&= \int_A E_T(y - y_c)x\mathrm{d}A - \tan(\alpha)\int_A E_T(y - y_c)y\mathrm{d}A \\
k_{22} &= \frac{\partial f_2}{\partial \phi_y} = \frac{\partial}{\partial \phi_y}\left[\int_A \sigma(\varepsilon(\phi_x, \phi_y))x\mathrm{d}A \right. \\
&\quad \left. -\tan\alpha \int_A \sigma(\varepsilon(\phi_x, \phi_y))y\mathrm{d}A\right] \\
&= \int_A \frac{\partial \sigma}{\partial \varepsilon}\frac{\partial \varepsilon}{\partial \phi_y}x\mathrm{d}A - \tan(\alpha)\int_A \frac{\partial \sigma}{\partial \varepsilon}\frac{\partial \varepsilon}{\partial \phi_y}y\mathrm{d}A \\
&= \int_A E_T(x - x_c)x\mathrm{d}A - \tan(\alpha)\int_A E_T(x - x_c)y\mathrm{d}A.
\end{aligned} \tag{37}$$

In this way, scaling the axial force through the load factor λ that is continuously adjusted, we can draw the complete N–M_x–M_y interaction diagram for a given bending moment's ratio. For a compression axial force, the iterative process is started with control in compression, whereas for a tension axial force the interaction diagrams are evaluated starting the iterative process imposing the failure of the cross-section in tension. Fig. 9 shows a simplified flowchart of this analysis algorithm. The algorithm is similar to that depicted in Fig. 7, but the initial values consist in the initial axial force N_0 and the angle α. The incrementation also starts with the curvatures $\phi_x = 0$ and $\phi_y = 0$.

It is important to note that, although this algorithm has been formulated for evaluating the interaction diagrams (N–M_x–M_y), by scaling the axial force through the load factor λ, the proposed algorithm can be easily modified in order to be applied to provide the moment capacity contour of the cross-sections (M_x vs. M_y). In this respect, the moment capacity contour can be evaluated by simply varying the angle α from 0 to 360° and solving system (32) for a given value of axial force N_0.

2.2.3. Moment capacity contour for given axial force N and bending moment M_x

In this case, injecting linear constraints (6) in nonlinear system (10), and arranging the system in accordance with the decoupled unknowns, we obtain:

$$\begin{cases} \displaystyle\int_A \sigma(\varepsilon(\phi_x, \phi_y))\mathrm{d}A - N_0 = 0 \\ \displaystyle\int_A \sigma(\varepsilon(\phi_x, \phi_y))y\mathrm{d}A - M_{x0} = 0 \\ \displaystyle\int_A \sigma(\varepsilon(\phi_x, \phi_y))x\mathrm{d}A - M_y = 0 \end{cases} \tag{38}$$

in which the bending moment M_y and the curvatures ϕ_x and ϕ_y represent the unknowns. Following a similar approach as presented above, the curvatures are obtained by solving the first two equations and then with this strain distribution the bending moment resistance about the y axis is computed with the last equation of the system.

Regarding the automatic drawing of the moment capacity contour, the strategy is as follows. Parametrizing the bending moment about x axis through the load factor λ and keeping the axial force constant $N = N_0$ and following a similar arc-length strategy as described in the case of interaction diagrams above, the complete moment capacity contour can be obtained, under constant axial force. Some particularities of implementation in this case have to be addressed. The solution procedures for the interaction diagrams have been based on the basic equations of equilibrium which implies a single loading vector proportionally scaled via load factor λ. In this case, maintaining the axial force N constant and scaling just the bending moment, we are in the situation of the non-proportionally applied loading, which involves two loading vectors, one that will be scaled and one fixed. The external loading can then be represented by:

$$\mathbf{f}^{\text{ext}} = \begin{bmatrix} N_0 \\ 0 \end{bmatrix} + \lambda \begin{bmatrix} 0 \\ M_{x0} \end{bmatrix} = \mathbf{f}^{\text{ext}}_{\text{fixed}} + \lambda \mathbf{f}^{\text{ext}}_{\text{scaled}} \tag{39}$$

so that the out-of-balance force vector becomes

$$\mathbf{F}(\lambda, \mathbf{\Phi}) = \mathbf{f}^{\text{int}} - \mathbf{f}^{\text{ext}}_{\text{fixed}} - \lambda \mathbf{f}^{\text{ext}}_{\text{scaled}} \tag{40}$$

and Eq. (18) then becomes

$$\delta\mathbf{\Phi} = -\mathbf{K}_T^{-1}\mathbf{F} + \delta\lambda \mathbf{K}_T^{-1}\mathbf{f}^{\text{ext}}_{\text{scaled}}. \tag{41}$$

With these relations the basic structure of the previous algorithms can be maintained. The iteration procedure is conducted with the tangent stiffness matrix computed as:

$$\mathbf{K}_T = \left(\frac{\partial \mathbf{F}}{\partial \mathbf{\Phi}}\right) = \begin{bmatrix} \dfrac{\partial f_1}{\partial \phi_x} & \dfrac{\partial f_1}{\partial \phi_y} \\ \dfrac{\partial f_2}{\partial \phi_x} & \dfrac{\partial f_2}{\partial \phi_x} \end{bmatrix} = \begin{bmatrix} k_{11} & k_{12} \\ k_{21} & k_{22} \end{bmatrix} \tag{42}$$

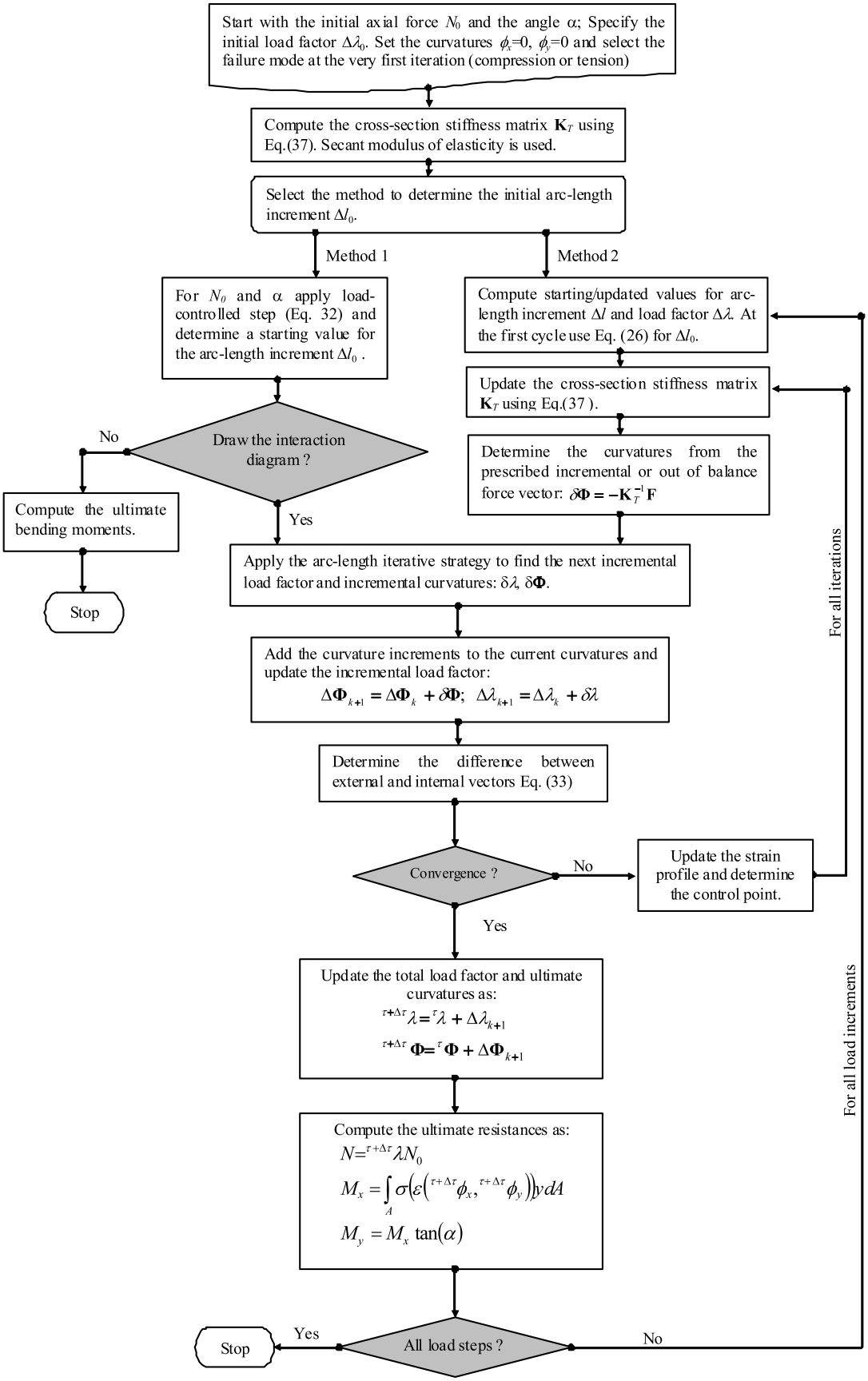

Fig. 9. Interaction diagrams for given bending moment's ratio and axial force. Analysis flowchart.

$$
\begin{aligned}
k_{11} &= \frac{\partial f_1}{\partial \phi_x} = \frac{\partial}{\partial \phi_x}\int_A \sigma(\varepsilon(\phi_x,\phi_y))\mathrm{d}A \\
&= \int_A \frac{\partial \sigma}{\partial \varepsilon}\frac{\partial \varepsilon}{\partial \phi_x}\mathrm{d}A = \int_A E_T(y-y_c)\mathrm{d}A \\
k_{12} &= \frac{\partial f_1}{\partial \phi_y} = \frac{\partial}{\partial \phi_y}\int_A \sigma(\varepsilon(\phi_x,\phi_y))\mathrm{d}A \\
&= \int_A \frac{\partial \sigma}{\partial \varepsilon}\frac{\partial \varepsilon}{\partial \phi_y}\mathrm{d}A = \int_A E_T(x-x_c)\mathrm{d}A \\
k_{21} &= \frac{\partial f_2}{\partial \phi_x} = \frac{\partial}{\partial \phi_x}\int_A \sigma(\varepsilon(\phi_x,\phi_y))y\mathrm{d}A \\
&= \int_A \frac{\partial \sigma}{\partial \varepsilon}\frac{\partial \varepsilon}{\partial \phi_x}y\mathrm{d}A = \int_A E_T y(y-y_c)\mathrm{d}A \\
k_{22} &= \frac{\partial f_2}{\partial \phi_y} = \frac{\partial}{\partial \phi_y}\int_A \sigma(\varepsilon(\phi_x,\phi_y))y\mathrm{d}A \\
&= \int_A \frac{\partial \sigma}{\partial \varepsilon}\frac{\partial \varepsilon}{\partial \phi_y}y\mathrm{d}A = \int_A E_T y(x-x_c)\mathrm{d}A
\end{aligned} \tag{43}
$$

$$
\begin{cases}
\displaystyle\int_A \sigma(\varepsilon(\phi_x,\phi_y))\mathrm{d}A - N_0 = 0 \\
\displaystyle\int_A \sigma(\varepsilon(\phi_x,\phi_y))y\mathrm{d}A - \lambda M_{x0} = 0.
\end{cases} \tag{44}
$$

The incremental-iterative procedure starts specifying the fixed bending moment M_{x0}, the fixed axial force N_0, the initial load increment $\Delta\lambda_0$ and initial arc-length increment Δl_0. However, the user will have little idea of an appropriate magnitude of the reference bending moment M_{x0} and the initial load factor. If the initial value of the bending moment is outside the moment capacity contour, this means that when the applied load combination (N_0, M_{x0}) exceeds the ultimate state condition of the cross-section, divergence of the iterative process will be signalled in this case. As in the previous procedures, the user may start by specifying a load increment $\Delta\lambda_0$ and then, the incremental curvature vector and the initial arc-length increment, can be determined by using Eqs. (25) and (26). Alternatively, a starting solution can be obtained as follows. Setting to zero one of the curvatures, for instance $\phi_y = 0$

$$\varepsilon(\phi_x) = \varepsilon_u + \phi_x(y - y_c) \tag{45}$$

and solving iteratively using the Newton scheme, for ϕ_x the first equation in system (44) we obtain

$$F(\phi_x) = \int_A \sigma(\varepsilon(\phi_x))\mathrm{d}A - N_0 = 0 \tag{46}$$

$$\phi_x^{k+1} = \phi_x^k - \frac{F(\phi_x^k)}{F'(\phi_x^k)} \tag{47}$$

$$\phi_x^{k+1} = \phi_x^k - \frac{\int_A \sigma(\varepsilon(\phi_x^k))\mathrm{d}A - N_0}{\int_A E_T(y-y_c)\mathrm{d}A}, \quad \phi_x^0 = 0, k \geq 0 \tag{48}$$

and then substituting this value in the second equation of system (44) we can compute the bending moment M_x as

$$M_{x0} = \int_A \sigma(\varepsilon(\phi_x))y\mathrm{d}A. \tag{49}$$

This value can be used as initial or starting value, which can be scaled with the loading parameter λ and the general arc-length procedure can be applied. Fig. 10 shows a simplified flowchart of this analysis algorithm.

2.3. Evaluation of tangent stiffness and stress resultant

Based on Green's theorem, the integration of the stress resultant and stiffness coefficients given by Eqs. (20), (37) and (43), over the cross-section will be transformed into line integrals along the perimeter of the cross-section. For this purpose, it is necessary to transform the variables first, so that the stress field is uniform in a particular direction, given by the current position of the neutral axis [19]. This is achieved by rotating the reference axes x, y to ξ, η oriented parallel to and perpendicular to the neutral axis, respectively (Fig. 2) such that:

$$\begin{cases} x = \xi\cos\theta + \eta\sin\theta \\ y = -\xi\sin\theta + \eta\cos\theta \end{cases} \tag{50}$$

where $\tan\theta = \phi_y/\phi_x$. Thus, the stress field is uniform in a direction parallel to the neutral axis, and strains, stresses and tangent modulus of elasticity can be expressed as a function of the single coordinate (η) as:

$$\varepsilon(\xi,\eta) = \varepsilon(\eta) = \varepsilon_0 + \phi\eta \tag{51}$$

$$\sigma(\varepsilon(\xi,\eta)) = \sigma(\varepsilon(\eta)) \tag{52}$$

$$E_T(\xi,\eta) = E_T(\eta) \tag{53}$$

where ϕ represents the total curvature $\phi = \sqrt{\phi_x^2 + \phi_y^2}$. This transformation is valid for a generic point of the cross-section. Therefore the stresses are calculated using the fiber strains, given by Eq. (9), and the assumed constitutive relations.

Based on this transformation, the internal forces carried by the compressive concrete and structural steel can be obtained by the following expressions:

$$
\begin{aligned}
N_{\mathrm{int}} &= \int\int \sigma(x,y)\mathrm{d}x\mathrm{d}y = \int\int \sigma(\eta)\mathrm{d}\xi\,\mathrm{d}\eta \\
M_{x,\mathrm{int}} &= \int\int \sigma(x,y)y\mathrm{d}x\mathrm{d}y \\
&= \int\int \sigma(\eta)(-\xi\sin\theta + \eta\cos\theta)\mathrm{d}\xi\,\mathrm{d}\eta \\
&= M_{\xi,\mathrm{int}}\cos\theta - M_{\eta,\mathrm{int}}\sin\theta \\
M_{y,\mathrm{int}} &= \int\int \sigma(x,y)x\mathrm{d}x\mathrm{d}y \\
&= \int\int \sigma(\eta)(\xi\cos\theta + \eta\sin\theta)\mathrm{d}\xi\,\mathrm{d}\eta \\
&= M_{\xi,\mathrm{int}}\sin\theta - M_{\eta,\mathrm{int}}\cos\theta
\end{aligned} \tag{54}
$$

where N_{int}, $M_{\xi,\mathrm{int}}$ and $M_{\eta,\mathrm{int}}$ are the internal axial force and bending moments about the ξ and η axis, respectively and can be obtained by the following expressions:

$$
\begin{aligned}
M_{\xi,\mathrm{int}} &= \int\int \sigma(\eta)\eta\mathrm{d}\xi\,\mathrm{d}\eta = \oint \sigma(\eta)\xi\eta\mathrm{d}\eta \\
M_{\eta,\mathrm{int}} &= \int\int \sigma(\eta)\xi\mathrm{d}\xi\,\mathrm{d}\eta = \frac{1}{2}\oint \sigma(\eta)\xi^2\mathrm{d}\eta \\
N_{\mathrm{int}} &= \int\int \sigma(\eta)\mathrm{d}\xi\,\mathrm{d}\eta = \oint \sigma(\eta)\xi\mathrm{d}\xi\,\mathrm{d}\eta.
\end{aligned} \tag{55}
$$

The tangent stiffness matrix coefficients are computed in the same way. For instance the coefficients given by Eq. (20) are evaluated based on the same transformation. Using the following notations:

$$
\begin{aligned}
s_1 &= \int\int_A E_T(\eta)\eta^2\mathrm{d}\xi\,\mathrm{d}\eta = \oint_L E_T(\eta)\eta^2\xi\mathrm{d}\eta \\
s_2 &= \int\int_A E_T(\eta)\xi^2\mathrm{d}\xi\,\mathrm{d}\eta = \frac{1}{3}\oint_L E_T(\eta)\xi^3\mathrm{d}\eta \\
s_3 &= \int\int_A E_T(\eta)\xi\eta\mathrm{d}\xi\,\mathrm{d}\eta = \frac{1}{2}\oint_L E_T(\eta)\xi^2\eta\mathrm{d}\eta \\
s_4 &= \int\int_A E_T(\eta)\eta\mathrm{d}\xi\,\mathrm{d}\eta = \oint_L E_T(\eta)\xi\eta\mathrm{d}\eta \\
s_5 &= \int\int_A E_T(\eta)\xi\mathrm{d}\xi\,\mathrm{d}\eta = \frac{1}{2}\oint_L E_T(\eta)\xi^2\mathrm{d}\eta
\end{aligned} \tag{56}
$$

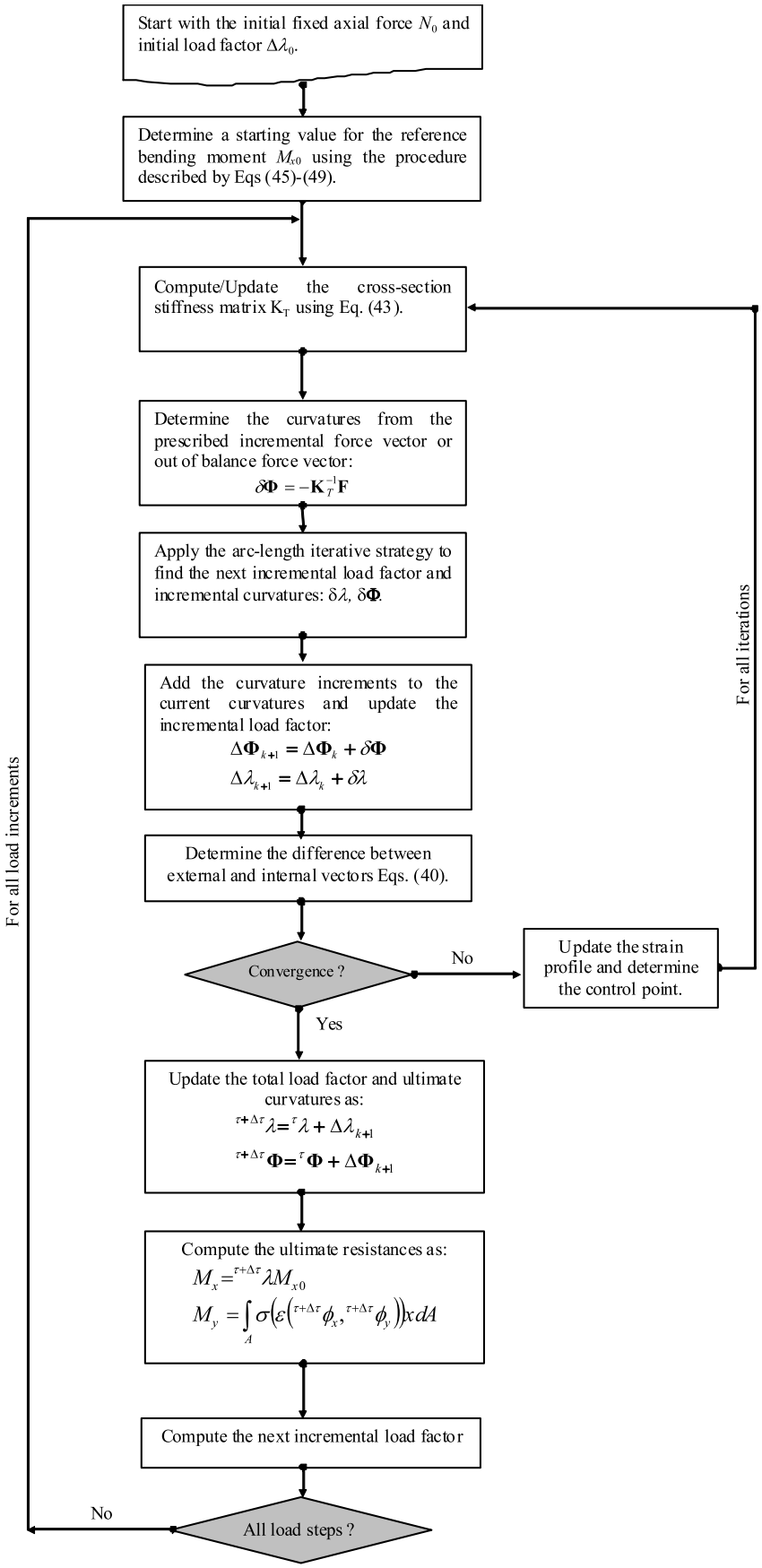

Fig. 10. Moment capacity contours for given axial force and bending moment M_x. Analysis flowchart.

the elements of the tangent stiffness matrix of the cross-section can be obtained as:

$$\begin{aligned} k_{11} &= S_1 - y_c S_4 \\ k_{12} &= S_3 - x_c S_4 \\ k_{21} &= S_3 - y_c S_5 \\ k_{22} &= S_2 - x_c S_5 \end{aligned} \tag{57}$$

$$\begin{Bmatrix} S_1 \\ S_2 \\ S_3 \\ S_4 \\ S_5 \end{Bmatrix} = \begin{bmatrix} c & -s & & & \\ s & c & & & \\ & & -2sc & c^2 & s^2 \\ & & c^2 - s^2 & sc & -sc \\ & & 2sc & s^2 & c^2 \end{bmatrix} \begin{Bmatrix} s_1 \\ s_2 \\ s_3 \\ s_4 \\ s_5 \end{Bmatrix} \tag{58}$$

where $c = \cos\theta$, $s = \sin\theta$ and A is the compressed region of the concrete or structural steel area, L is the perimeter of this region, $\sigma(\eta)$ and $E_T(\eta)$ are the stress and tangent elasticity modulus of deformation of the fiber η, respectively. In the same way the tangent stiffness matrix coefficients (given by Eqs. (37) and (43), respectively) can be obtained.

As the integration area contour is approximated by a polygon, the integral over the perimeter L, can be obtained by decomposing this integral side by side along the perimeter:

$$\oint_L h(\eta)\xi^p \mathrm{d}\eta = \sum_{i=1}^{nL} \int_{\eta_i}^{\eta_{i+1}} h(\eta)\xi^p \mathrm{d}\eta \tag{59}$$

where nL is the number of sides that forms the integration area. The sides are defined by the $\xi\eta$ coordinates of the endpoints as shown in Fig. 2. When the integration area is a circle with radius R, the integral over the perimeter L can be obtained by decomposing this integral as [19]:

$$\begin{aligned} \oint_L h(\eta)\xi^p \mathrm{d}\eta = &\int_{-R}^{R} h(\eta)(R^2 - \eta^2)^{p/2} \mathrm{d}\eta + (-1)^p \\ &\times \int_{R}^{-R} h(\eta)(R^2 - \eta^2)^{p/2} \mathrm{d}\eta. \end{aligned} \tag{60}$$

This leads to a significant saving in imputing the data to describe the circular shapes, without the need to decompose the circular shapes as a series of straight lines and approximate the correct solution when circular boundaries are involved.

In order to perform the integral on a determined side of the contour (L_i), polygonal or circular, of the integration area, the interpolatory Gauss–Lobatto method is used. Though this rule has lower order of accuracy than the customary Gauss–Legendre rule, it has integration points at each end of the interval, and hence performs better in detecting yielding. When there is no transition point of piecewise stress–strain diagrams, n integration points integrate exactly a polynomial of order $(2n - 3)$. For a second-degree parabola, as commonly used for the stress–strain curve of concrete in compression, three Gauss–Lobatto integration points are necessary. However, because the stress field is defined by a piecewise function (i.e. a second-degree parabola, for ascending part, and a straight line for descending part) and there is no continuity in the derivative, the polynomial interpolation can produce important integration errors [9]. Although the integration methods proposed in [13,20] are "exact" even in the presence of transition points, these methods require a significant computational cost. In the proposed approach, an adaptive quadrature strategy is used. This procedure combined with the Gauss–Lobatto integration rule can be applied successfully as follows: Start by dividing the interval into two, and use the quadrature rule in each subinterval. Then compare the results with the same quadrature rule applied to the whole interval under consideration. If the difference is smaller than a given tolerance, there is no need to refine. Otherwise, repeat this procedure, recursively, with each individual interval. In this paper, the tolerance adopted to stop the refinement of the interval has been taken as 1E−5 in all computational examples. In this context of adaptivity quadratures, the Lobatto integration scheme has another advantage over the Legendre integration scheme, given by the fact that the point corresponding to the left end in one interval is the same as the point corresponding to right end in the next. So, assuming that we keep the values of the integrand at the interval endpoints after we have evaluated them and reuse them where appropriate, the cost of evaluating a Lobatto rule is reduced by about one integrand evaluation compared with Legendre rule.

The contribution of the steel reinforcement bars does not present computational difficulties. The steel bars are assumed to be discrete points with area A_{sj}, coordinates x_{sj}, y_{sj} and stress f_{sj}. The total steel axial force and bending moment resultants are:

$$\begin{aligned} N_s &= \sum_{i=1}^{N_b} A_{sj} f_{sj}, \qquad M_{xs} = \sum_{i=1}^{N_b} y_{sj} A_{sj} f_{sj}, \\ M_{ys} &= \sum_{i=1}^{N_b} x_{sj} A_{sj} f_{sj} \end{aligned} \tag{61}$$

and to avoid double counting of the concrete area that is displaced by the steel bars, the force $A_{sj}f_{cj}$ is subtracted from the reinforcement bar force $A_{sj}f_{sj}$, where $A_{sj}f_{cj}$ is the concrete compressive stress at the centroid of the reinforcement bar.

Furthermore, in order to identify the various regions in a complex cross-section with different material properties (confined or unconfined concrete, structural steel) each region with assigned material properties is treated separately. Two material properties are defined [13]: the "foreground" material and the "background" material. The "foreground" material is taken into account with a positive sign, whereas the "background" material is taken into account with a negative sign, and then each region is treated as separate cyclic summations. In this way, any composite cross-section with different material properties can be integrated without difficulties.

3. Computational examples

Based on the analysis algorithm just described, a computer program **ASEP** has been developed to study the biaxial strength behaviour of arbitrary concrete–steel cross-sections. It combines the analysis routine with a graphic routine to display the final results (Fig. 11). The computational engine was written using Compaq Visual Fortran. The graphical interface was created using Microsoft Visual Basic 6. Dynamic Link Libraries (DLL) are used to communicate between the interface and engine. The many options included make it a user friendly computer program. The graphical interface allows for easy generation of cross-sectional shapes and reinforcement bars, graphical representation of the data, and plotting of the complete stress field over the cross-section, instantaneous position of neutral axis, interaction and moment capacity contour diagrams, etc.

The accuracy and computational advantages of the numerical procedure developed here has been evaluated by using two selected benchmark problems analysed previously by other researchers by using different numerical or experimental methods. In all computational examples, the equilibrium tolerance has been taken as 1E−7 and the stress–strain curve of concrete under compression is represented by a combination of a second-degree parabola (for ascending part) and a straight line (for descending part). The concrete tensile strength is neglected. A bilinear elasto-plastic stress–strain relationship for the reinforcement bars and structural steel, both in tension and in compression, is assumed.

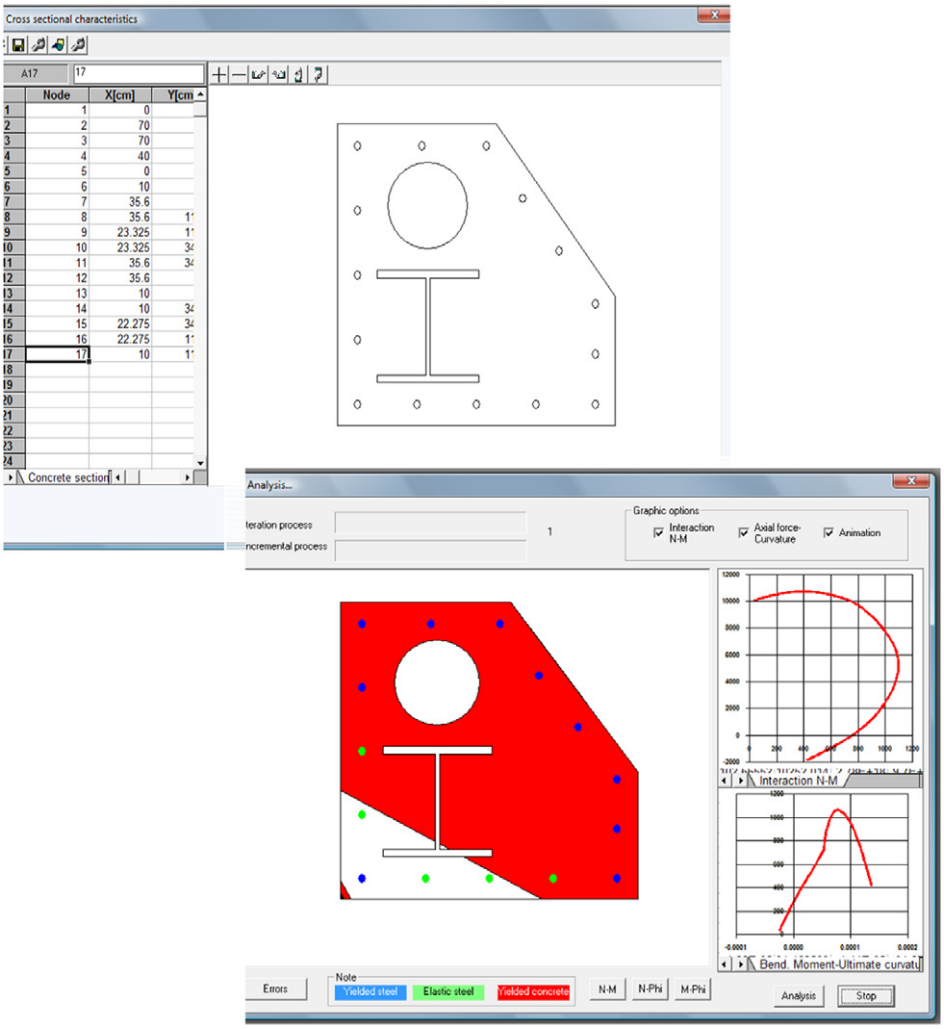

Fig. 11. ASEP screen-shots.

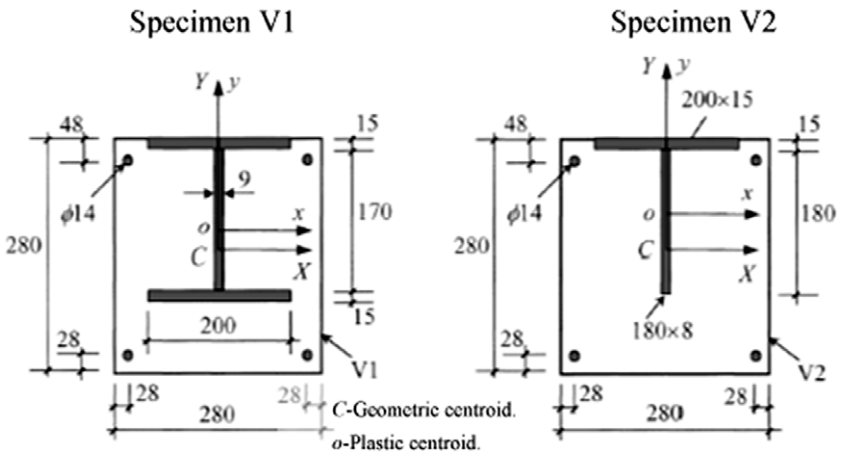

Fig. 12. Example 1. Rectangular cross-sections with asymmetrically placed structural steel.

3.1. Example 1: rectangular cross-section with asymmetrical structural steel

In order to evaluate the validity, accuracy and convergence of the proposed procedure, the interaction diagrams and moment capacity contours of two rectangular cross-sections with asymmetrically placed structural steel under biaxial loading are determined and compared with the available experimental tests [21] and with the numerical procedure developed in [7]. The cross-sections consist of a concrete core and two asymmetrically placed I shaped or T shaped structural steel (Fig. 12). The cross-sections have been experimentally tested under uniaxial loading by Roik and Bergman [21], and further studied analytically by Chen et al. [7]. Characteristic strength for concrete in compression is $f_c = 31.79$ MPa and the stress–strain curve which consists of a parabolic and a linear part was used in the calculation, with

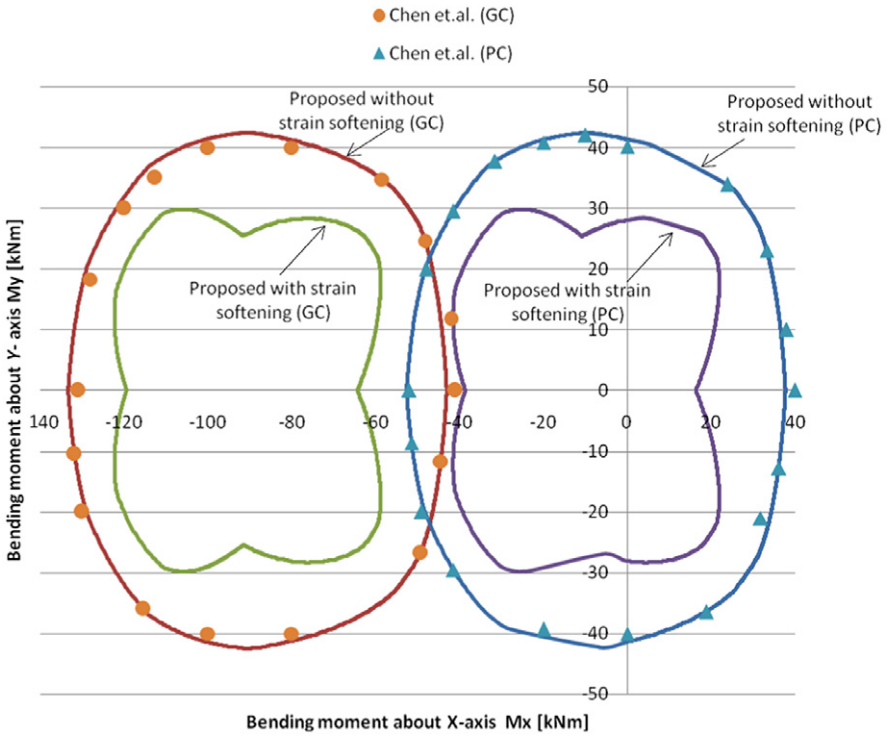

Fig. 13. Moment capacity contours of section $V2$ with compressive axial load $N = 3000$ kN.

crushing strain $\varepsilon_0 = 0.002$ and ultimate strain $\varepsilon_{cu} = 0.0035$. In the work of Chen et al. [7] the strain softening of concrete in compression has been ignored, but in the current work this effect can be taken into account through the parameter γ (see Eq. (2)). Young's modulus for all steel sections was 200 GPa while the maximum strain was assumed to be $\varepsilon_{su} = \pm 1\%$. The yield strength of the steel reinforcing bars is $f_y = 420$ MPa, whereas for the structural steel the following values have been considered. For specimen $V1$ (Fig. 12) the yield strength of the flange is $f_{y,\text{flange}} = 206$ MPa and that of the web steel is $f_{y,\text{web}} = 220$ MPa; for specimen $V2$ the yield strength of the flange is $f_{y,\text{flange}} = 255$ MPa and that of the web steel is $f_{y,\text{web}} = 239$ MPa.

These examples can be considered as "convergence patch tests". For the majority of the numerical algorithms, the convergence of the iterative process cannot be guaranteed when the magnitude of the axial load approaches the axial load capacity and when the geometric centroid of the cross-section is chosen as the origin of the reference axis [7]. For these situations Chen [7] suggested that the plastic centroid [21] of the cross-section has to be chosen as the origin of the reference axes. In order to verify the robustness of the algorithms developed in the current paper, the cross-section $V2$ has been analysed, drawing the interaction diagrams and moment capacity contours for axial loads near the pure compression state (for $\gamma = 0$, $N_{\text{comp}} = 3699.2$ kN) or pure tension state ($N_{\text{tension}} = -1367.6$ kN), considering both geometric and plastic centroids of the cross-section. Convergence problems have been experienced by Chen [7] in this portion of the moment capacity contour when the geometrical centroid of the cross-section has been taken as the origin of the reference loading axes.

Fig. 13 presents the moment capacity contours, obtained by the algorithm proposed in Section 2.3, and those obtained by Chen [7], for the cross-section $V2$ for the compressive axial load $N = 3000$ kN, considering as reference loading axes, geometric centroid (GC) and plastic centroid (PC), respectively [7]. No convergence problems have been experienced by the proposed approach, even when the geometric centroid has been chosen as reference axes or the strain softening of the concrete in compression has been taken into account ($\gamma = 0.15$), a maximum of three iterations have been required to complete the entire interaction diagram.

As can be seen, the results obtained in the current paper and those reported in [7] agree closely in both cases. However it is important to note that, the method proposed by Chen does not generate genuinely plane moment capacity curves. The method proposed in [7] fails in some circumstances to draw the moment capacity contour, under a fixed axial load, and in order to overcome some divergences, the axial load value is slightly adjusted. Furthermore, based on the proposed approach, the moment capacity contour of the cross-section has been determined, without any convergence difficulties, even for axial loads approaching the axial load capacity under pure compression.

Fig. 14 presents the moment capacity contours, obtained by the proposed algorithm, ignoring the strain softening effect of the concrete in compression, for different magnitudes of axial loads. As noted by Chen [7] if the geometric centroidal axes are taken as the reference loading axes, the origin of the axes falls outside the moment capacity contour. This effect is more accentuated as axial load approaches axial load capacity under pure compression and can be clearly observed in Fig. 14.

Fig. 15 presents the moment capacity contours for the case when the strain softening effect of the concrete is modelled; a maximum of five iterations have been required to complete the entire interaction diagram for a compressive axial load of 3500 kN. For these cases, Ref. [7] does not present comparative results.

Fig. 16 shows the complete interaction diagrams under uniaxial bending moment about x axis with and without the effect of the strain softening of concrete. As can be seen, near the compressive axial load capacity multiple solutions exist in the N–M space when the strain softening is modelled. For these points the strain field fulfils the ultimate value for concrete in compression. The lack of uniqueness of the solution, when the strain softening is taken into account, can be also observed on the moment–ultimate curvature diagrams (Fig. 17), when multiple "snap-through" phenomena occur in these situations. Therefore, the proposed approach

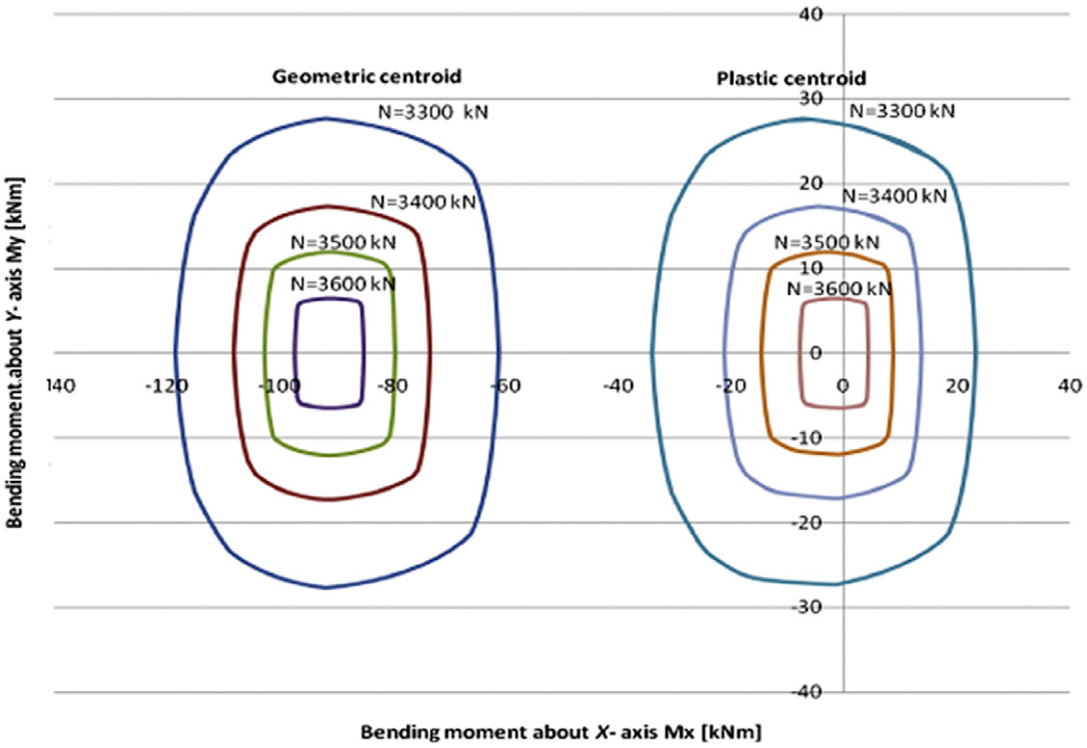

Fig. 14. Moment capacity contour of section *V*2 for different values of compressive axial load. Strain softening ignored.

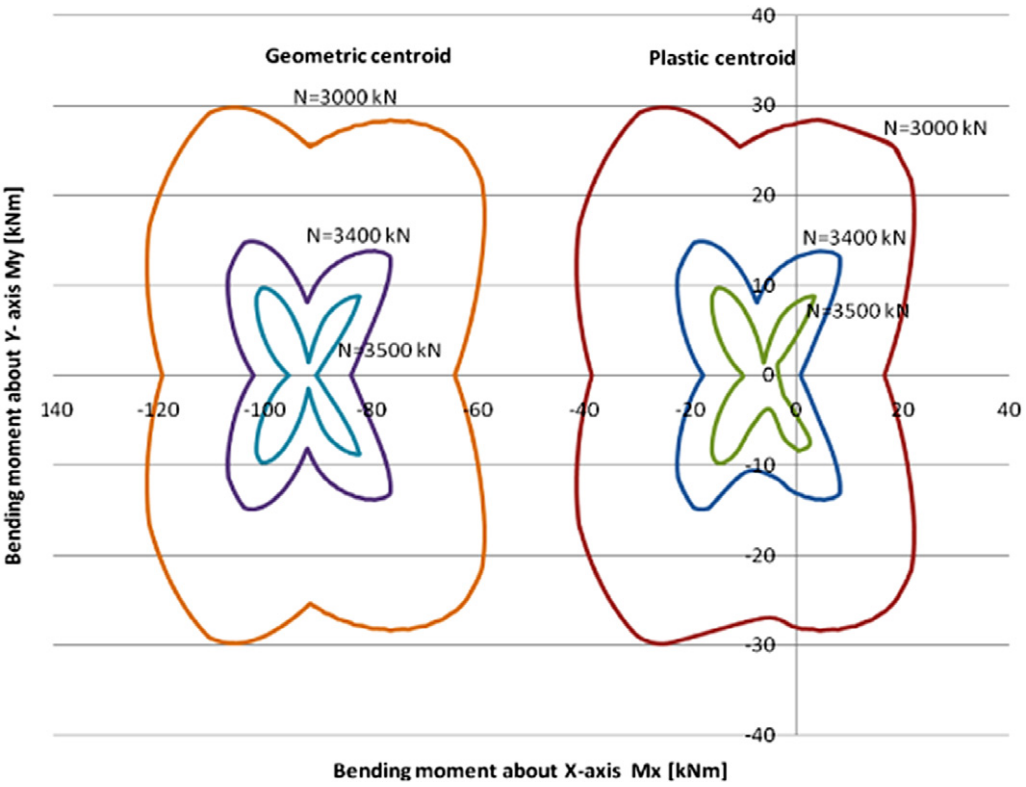

Fig. 15. Moment capacity contour of section *V*2 for different values of compressive axial load. Strain softening included.

based on arc-length constraint strategy is essential to assure the convergence of the entire process and to determine all possible solutions; a maximum of three iterations have been required to complete the entire interaction diagram. When the strain softening is ignored ($\gamma = 0$), the moment–ultimate curvature curve is flat in that region (Fig. 17) and this explains the uniqueness of the solution in the N–M space in this case Fig. 16. Furthermore, the effects of confinement in the concrete were investigated for different values of degree of confinement. As can be seen in Fig. 18, by reducing the confinement in the concrete the interaction curves

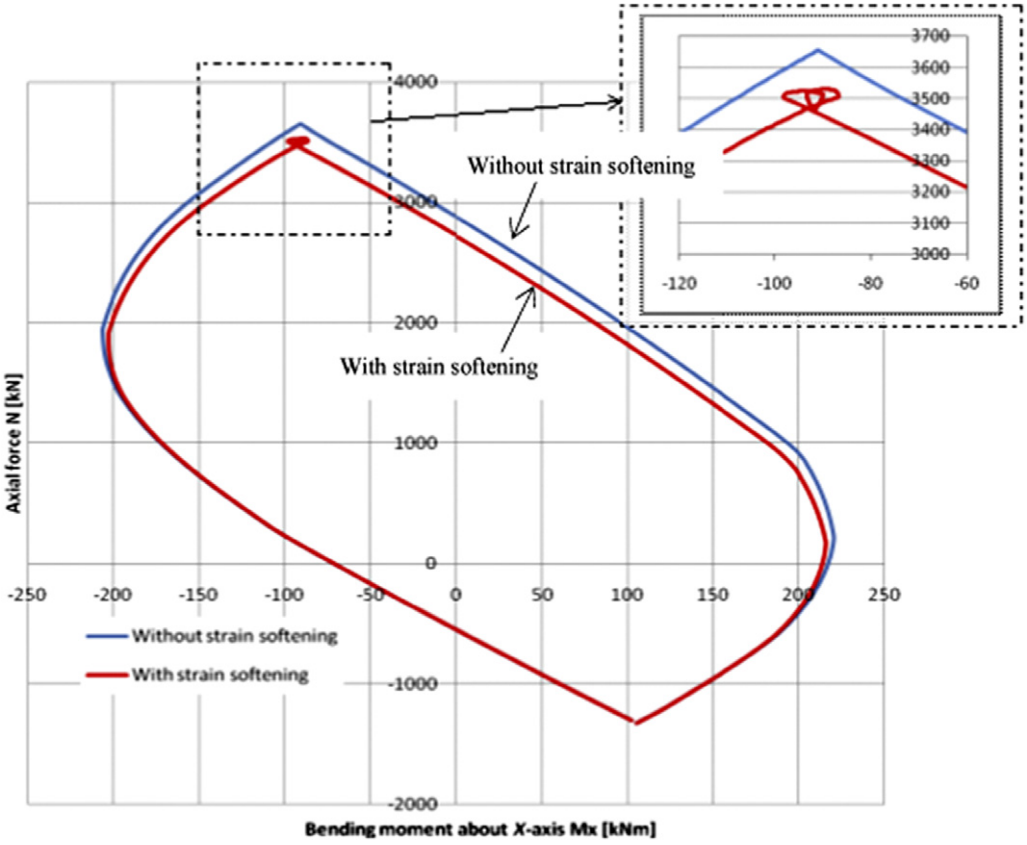

Fig. 16. Interaction diagrams under uniaxial bending moment about *x* axis.

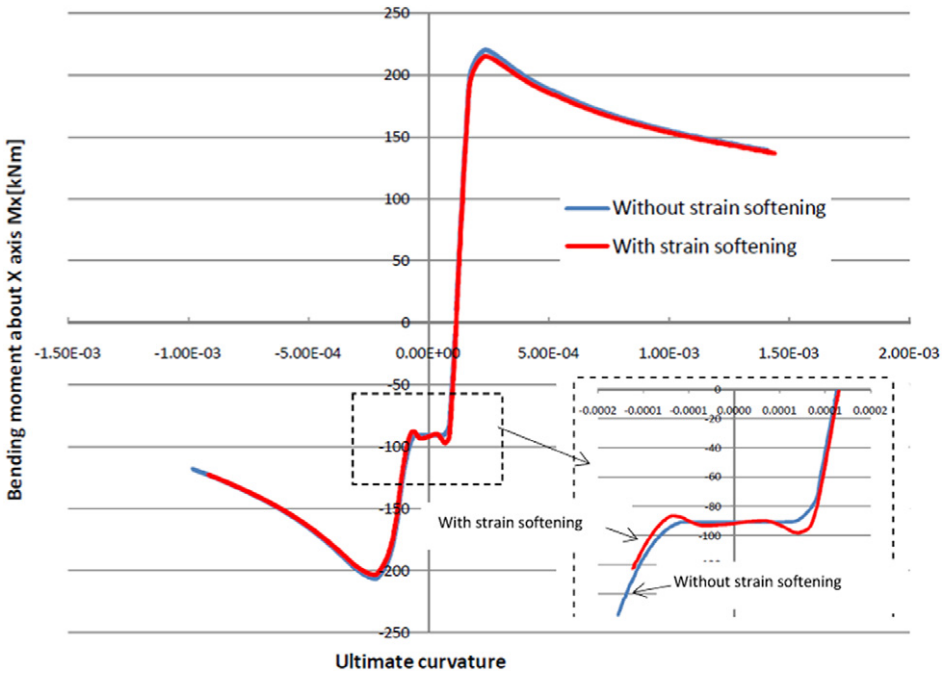

Fig. 17. Bending moment–ultimate curvature variation for *V*2 cross-section.

indicate lower capacities and the non-convexity of the diagrams is more pronounced.

Fig. 19 presents the moment capacity contours, obtained by the proposed algorithm, when the section is subjected to tensile axial forces near the ultimate limit. These diagrams are computed about the geometric centroidal axes of the cross-section. No convergence problems have been experienced, but in these cases a higher number of iterations have been required to complete the diagrams. For instance, for a tensile axial force of $N = -1250$ kN, a maximum of 18 iterations have been required to establish the equilibrium.

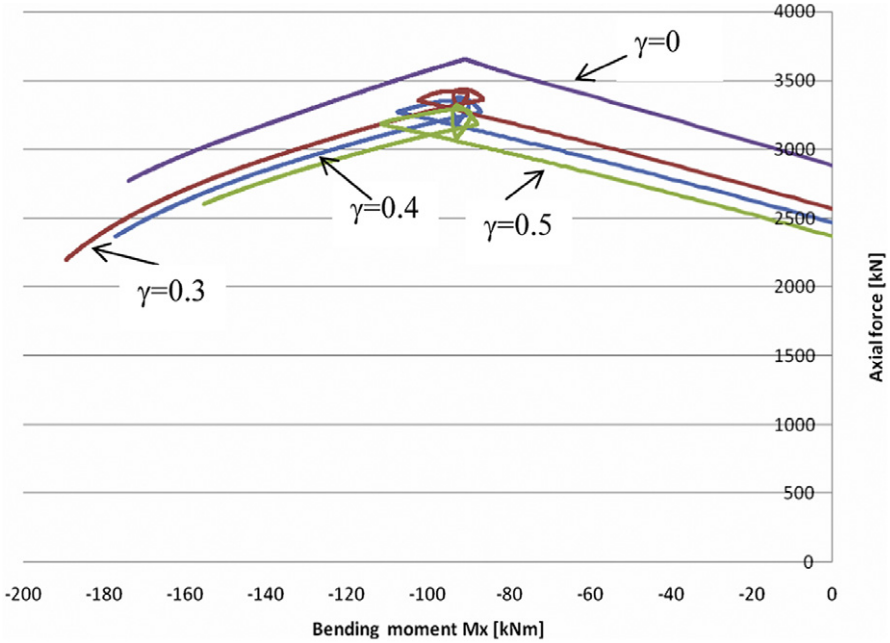

Fig. 18. Interaction diagram *N–Mx* for different values of degree of confinement.

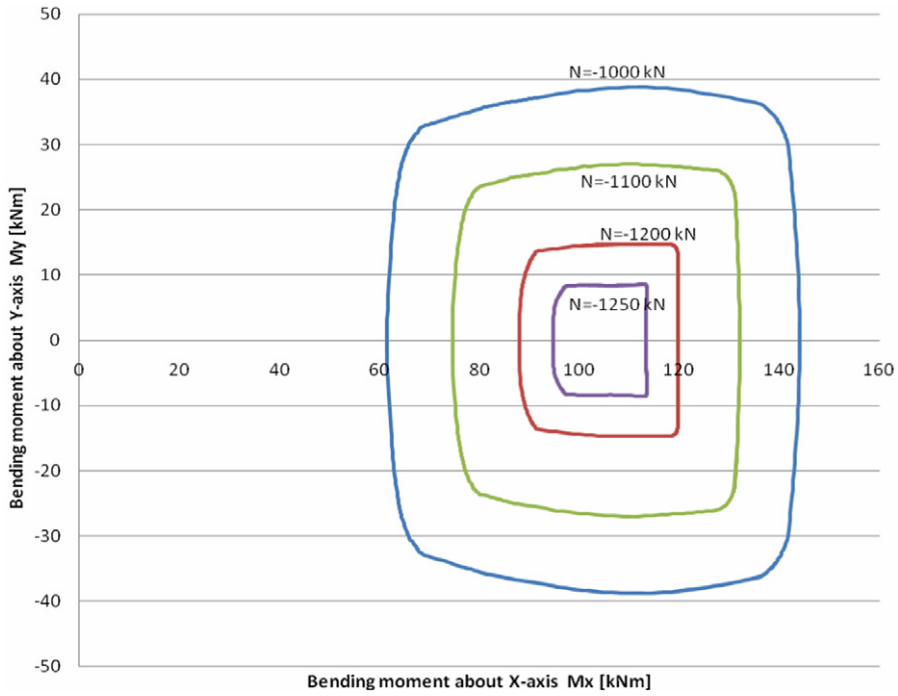

Fig. 19. Moment capacity contour of section *V2* for different values of tensile axial load.

The effects of confinement in the concrete are shown by the moment capacity diagrams of Fig. 20. These diagrams are evaluated for a compressive axial load of $N = 3000$ kN and different values of degree of confinement γ. As can be seen, by reducing the confinement in concrete (i.e. by increasing the value of γ) the interaction curves indicate lower capacities and the non-convexity of the diagrams is more pronounced. No convergence problems have been encountered even for $\gamma = 0.4$, a maximum of seven iterations have been required to complete the interaction diagram in this case.

Fig. 21 shows the comparative interaction diagrams for $\alpha = 15^\circ$ and 30°, respectively. The bending moments are computed about axes *x–y*, which pass through the geometric centroid of the cross-section.

In order to prove the ability of the proposed approach to compute directly the ultimate resistance of the cross-section, when one of the components of the section forces is known, and to compare the present results with the experimental tests, the results reported in [21] are compared with those obtained by the present approach and those reported in [7]. The load-carrying capacities of the cross-sections under different eccentricities reported in [21] are compared with those computed by the present approach, assuming that the axial forces are determined experimentally in [21] as ultimate resistances for different eccentricities. These values have been considered as

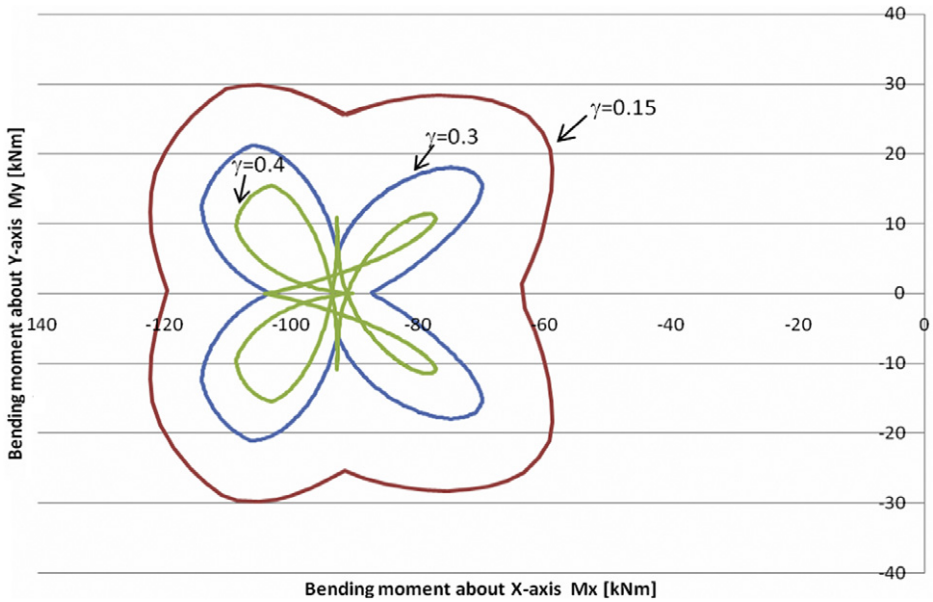

Fig. 20. Moment capacity contours of section $V2$ with compressive axial load $N = 3000$ kN for different values of the degree of confinement γ.

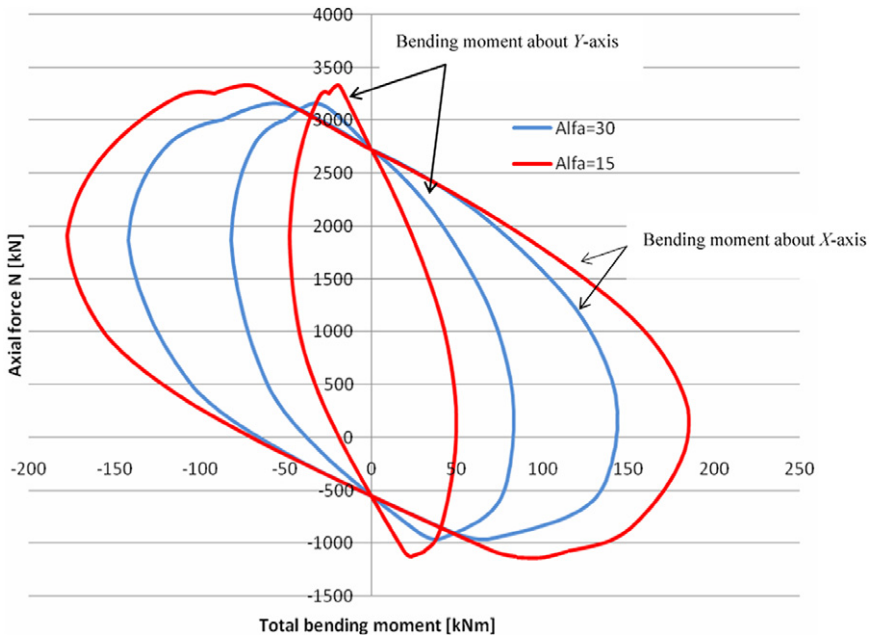

Fig. 21. Biaxial interaction diagrams for $V2$ cross-section.

Table 1
Example 1: load-carrying capacities and comparison with test results.

Specimen		Chen. et al. [7]		Experimental test [21]		Present paper	
		N (kN)	M_x (kN m)	N (kN)	M_x (kN m)	N (kN)	M_x (kN m)
V1	$e_y = 0$	3608	0	3617	0	3617	0.54
	$e_y = -40$	2654	−106.16	2825	−113	2825	−109.25
	$e_y = 100$	1937	193.7	1800	180	1800	190.2
V2	$e_y = 0$	2880	0	2654	0	2654	0.33
	$e_y = -40$	2107	−84.28	1998	−79.92	1998	−82.53
	$e_y = 100$	2036	203.6	1706	170.6	1706	178.25

initial values in the algorithm described in Section 2.2.2 and the associated bending moments have been computed. Table 1 gives the computed load-carrying capacities of the six specimens and the comparison with the test results and those reported in [7]. As can be seen the present values agree closely with test results.

Table 2
Example 2: failure surface points computed for given bending moments.

M_x (kN m)	M_y (kN m)	N (kN)	Number of iterations	Failure mode at first iteration (compression or tension)
10	2.68	9 997.27	6	Compression
10	−2.68	9 970.53	6	Compression
800	373	1 558.23	5	Compression
600	−280	8 162.18	3	Compression
600	280	10 407.45	4	Compression
600	280	−670.37	5	Tension
800	214.35	530.53	3	Tension
−86	−23	−3 863.11	6	Tension
−541	−145	−4 261.17	7	Tension
−600	−280	−4 159.35	4	Tension

3.2. Example 2: composite steel–concrete cross-section with arbitrary shape

The composite steel–concrete cross-section depicted in Fig. 22, consists of the concrete matrix, fifteen reinforcement bars of diameter 18 mm, a structural steel element and a circular opening. Characteristic strengths for concrete, structural steel and reinforcement bars are $f_c = 30$ MPa, $f_{st} = 355$ MPa and $f_s = 460$ MPa, respectively. These characteristic strengths are reduced by dividing them with the corresponding safety factors $\gamma_c = 1.50$, $\gamma_{st} = 1.10$ and $\gamma_s = 1.15$. The stress–strain curve for concrete which consists of a parabolic and linear-horizontal part was used in the calculation, with the crushing strain $\varepsilon_0 = 0.002$ and ultimate strain $\varepsilon_{cu} = 0.0035$. Young's modulus for all steel sections was 200 GPa while the maximum strain was $\varepsilon_u = \pm 1\%$. The strain softening effect for the concrete in compression is taken into account, in the present approach, through the parameter γ. This is an example proposed and analysed by Chen et al. [7] and later studied by Charalampakis and Koumousis [13], Rosati et al. [11] and others. The moment capacity contours (M_x–M_y interaction curve) have been determined under a given axial load $N = 4120$ kN using the approach described in Section 2.3 and compared with the results reported in [7], Fig. 23. As can be seen the results are in close agreement when the bending moments are computed about the plastic centroidal axes of the cross-section. However, as was mentioned previously, the method proposed by Chen [7] does not generate genuinely plane moment capacity curves, because of convergence problems caused by the fixed axial force. On the contrary, with the proposed approach, the interaction curve can be computed without any convergence difficulties; a maximum of three iterations are necessary to establish the equilibrium, even when the geometric centroid has been chosen as the origin of the reference axes or the strain softening of the concrete in compression is taken into account ($\gamma = 0.15$). The moment capacity curves for these situations are also depicted in Fig. 23. For these cases, Ref. [7] does not present comparative results.

Charalampakis and Koumousis [13] also analysed this section using a method based on isogonic curves. Running the present computer program on a laptop computer with 2 GHz processor, the entire moment capacity diagram has been determined in about 4 s, which is almost 1.5 times shorter than the time taken to complete the same analysis with the computer program of Charalampakis and Koumousis [13]. Moreover the moment capacity curve determined in the current approach contains 533 points whereas the interaction curve in [13] has been determined with 10° angle step requiring 36 points in total to complete the same interaction curve. This demonstrates the time saving of the proposed numerical method. In order to verify the stability of the proposed method a series of analyses have been conducted to determine the interaction curves for different values of bending moment's ratio $M_y/M_x = \tan(\alpha)$. The bending moments are computed about the geometric centroidal axes of the cross-section and the strain softening of the concrete in compression has been

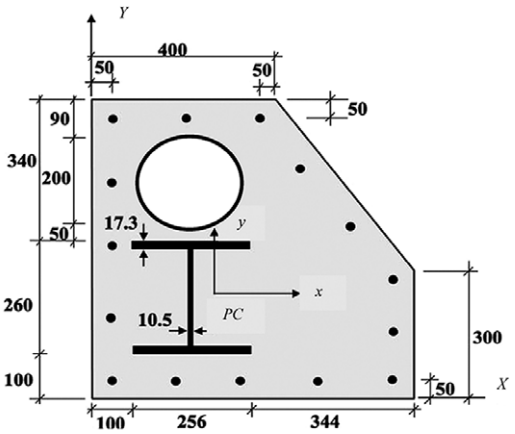

Fig. 22. Example 2. Composite steel–concrete cross-section.

modelled ($\gamma = 0.15$). Figs. 24 and 25 shows the interaction diagrams for $\alpha = 0°$, 30°, 60°, 90°. No convergence problems have been encountered using the proposed approach; a maximum of three iterations have been required to complete the entire interaction diagram in each case.

In the analyses conducted by Rosati et al. [11] the ultimate load capacity of this cross-section has been evaluated using a method which solves the equilibrium equations and impose the ultimate limit at the same time. The interaction curves in [11] have been determined by considering twelve pairs (M_x, M_y) for each value of the axial force. The strain softening of concrete in compression has been ignored. Using the proposed approach the moment capacity contours have been determined for different values of axial loads approaching the axial load capacity under pure compression and tension. Fig. 26 presents the moment capacity contours, obtained by the algorithm proposed in Section 2.2.3, and those reported by Rosati et al. [11]. As can be seen the results are in close agreement. No convergence problems have been encountered using the proposed approach; under the equilibrium tolerance of 1E−7 a maximum of four iterations have been required to complete the entire moment capacity diagrams for each case of compression whereas a maximum of six iterations have been required to establish the equilibrium for each case of tension. This comparison illustrates the accuracy of the proposed approach and convergence stability.

In order to prove the ability of the proposed approach to compute directly the ultimate resistances of the cross-section and to evaluate the convergence behaviour, Tables 2 and 3 report several points of the failure surface determined by the algorithms described in Sections 2.2.1 and 2.2.2, respectively. Table 2 presents the computed axial force resistances for given bending moments, whereas Table 3 reports the computed bending moments for a given bending moment's ratio and axial force. The strain softening effect for the concrete in compression is not taken into account. The load-controlled method enhanced with an adaptive-descent

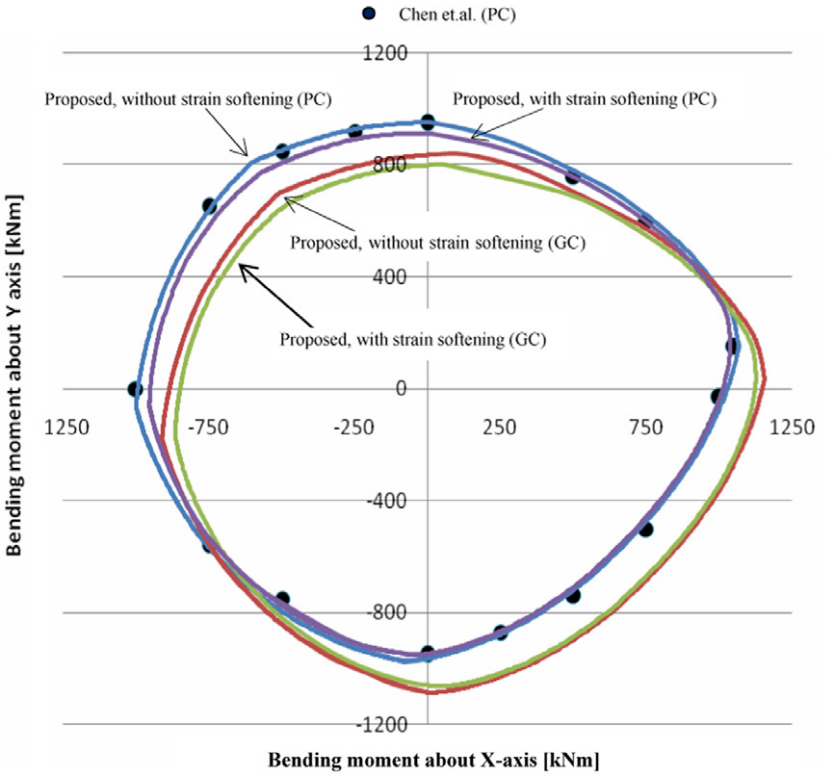

Fig. 23. Moment capacity contour with axial load $N = 4120$ kN.

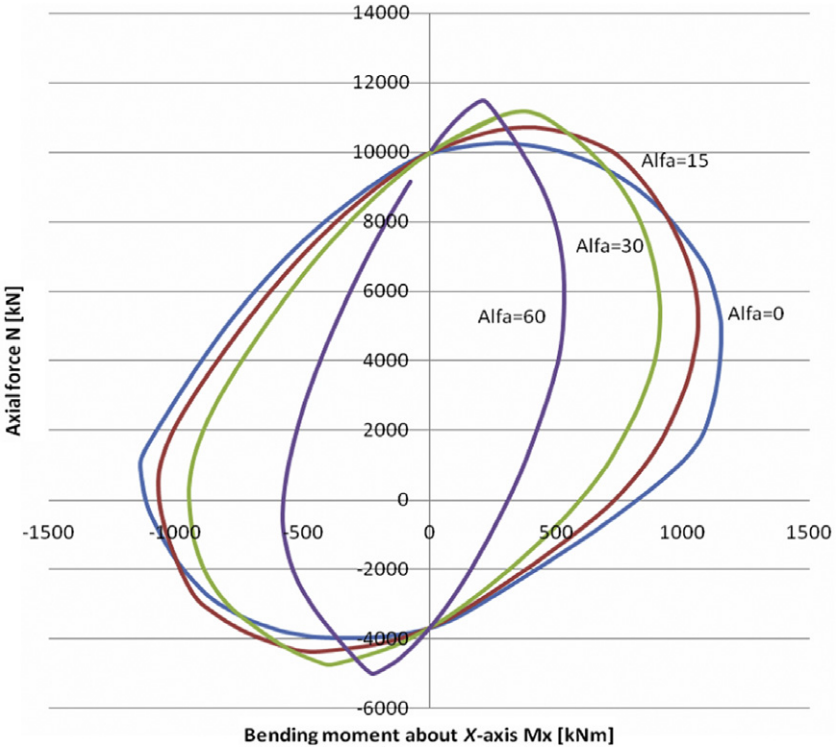

Fig. 24. Biaxial interaction diagrams. Bending moments about x axis.

strategy, as described herein, has been applied. As can be seen, a low number of iterations have been required to establish the equilibrium, despite the fact that, in all cases, the iterative process has been started with curvatures $\phi_x = 0$ and $\phi_y = 0$, and a very restrictive equilibrium tolerance (i.e tol = 1E−7), has been considered.

4. Conclusions

A new computer method based on incremental-iterative arc-length technique has been presented for the ultimate strength analysis of composite steel–concrete cross-sections subjected to axial force and biaxial bending. Comparing the algorithm

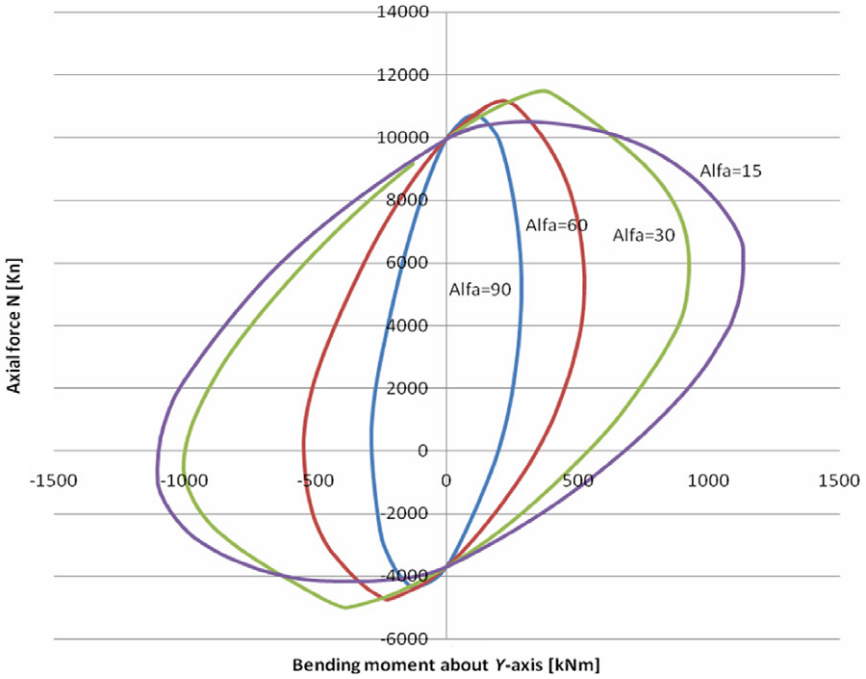

Fig. 25. Biaxial interaction diagrams. Bending moments about *y* axis.

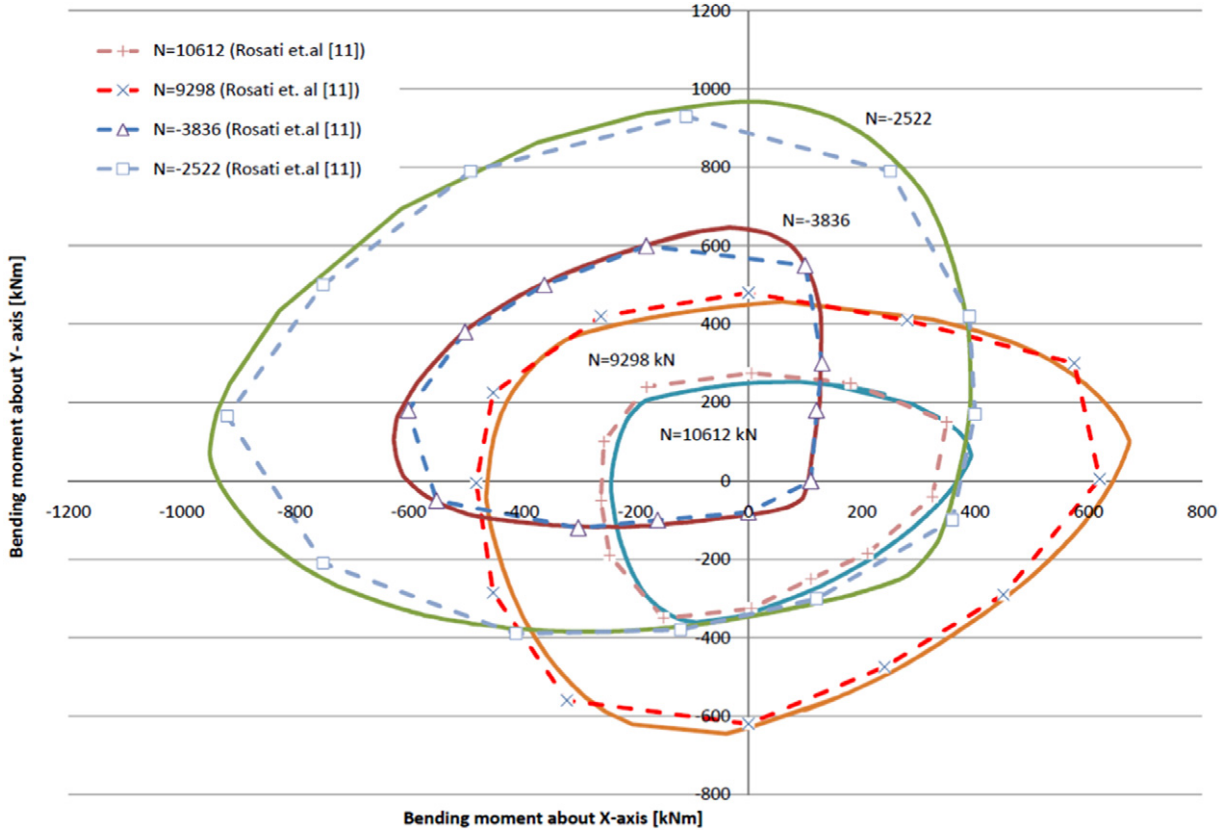

Fig. 26. Moment capacity contours for different values of axial load.

presented in the current paper with the existing methods, it can be concluded that the proposed approach is general, can determine both interaction diagrams and moment capacity contours, and, of great importance, it is fast, the diagrams are directly calculated by solving, at a step, just two coupled nonlinear equations. Convergence is assured for any load case, even near the state of pure compression or tension and is not sensitive to the initial/starting values, to how the origin of the reference loading axes is chosen or to the strain softening effect for concrete in compression. Furthermore, the proposed method can be applied to provide directly the ultimate resistance of the cross-section, in the hypothesis that one or two components of the section forces are known, without the need of knowing in advance the whole interaction diagram or moment capacity contour. An object

Table 3
Example 2: failure surface points computed for given bending moment's ratio and axial force.

N (kN)	α (deg)	M_x (kN m)	M_y (kN m)	Number of iterations
5940	30	906.91	523.60	4
5940	15	1054.21	282.47	5
7920	45	685.35	685.35	6
7920	225	−258.98	−258.98	6
4950	195	−740.22	−198.34	3
3960	210	−744.43	−429.79	5
−4257	205	−216.50	−100.95	7
−2970	15	181.36	48.6	5
−495	15	657.76	176.24	5

oriented computer program with full graphical interface was developed to obtain the interaction diagrams and moment capacity contours of composite cross-sections under combined biaxial bending and axial load. The method has been verified by comparing the predicted results with the established results available from the literature. It can be concluded that the proposed numerical method proves to be reliable and accurate for practical applications in the design of composite steel–concrete beam–columns and can be implemented in the advanced analysis techniques of three-dimensional composite frame structures. Future work is envisaged to investigate various effects such as concrete tensile strength and residual stresses of structural steels on the ultimate strength behaviour of composite steel–concrete cross-sections or arbitrary shape.

Acknowledgements

The author gratefully acknowledges the support from Romanian National Authority for Scientific Research (ANCS and CNCSIS-Grant PNII-IDEI No. 193/2008) for this study. The author would also like to thank the anonymous reviewers for their comments and suggestions to improve the manuscript.

References

[1] Chiorean CG, Barsan GM. Large deflection distributed plasticity analysis of 3D steel frameworks. Comput Struct 2005;83(19–20):1555–71.
[2] Izzudin BA, Lloyd Smith D. Efficient nonlinear analysis of elasto-plastic 3D R/C frames using adaptive techniques. Comput Struct 2000;78:549–73.
[3] Rotter JM. Rapid exact inelastic biaxial bending analysis. J Struct Eng, ASCE 1985;111(12):2659–67.
[4] De Vivo L, Rosati L. Ultimate strength analysis of reinforced concrete sections subject to axial force and biaxial bending. Comput Methods Appl Mech Engrg 1998;166:261–87.
[5] Rodrigues JA, Aristizabal-Ochoa JD. Biaxial interaction diagrams for short RC columns of any cross section. J Struct Eng, ASCE 1999;125(6):672–83.
[6] Fafitis A. Interaction surfaces of reinforced-concrete sections in biaxial bending. J Struct Eng, ASCE 2001;127(7):840–6.
[7] Chen SF, Teng JG, Chan SL. Design of biaxially loaded short composite columns of arbitrary section. J Struct Eng, ASCE 2001;127(6):678–85.
[8] Sfakianakis MF. Biaxial bending with axial force of reinforced, composite and repaired concrete cross sections of arbitrary shape by fiber model and computer graphics. Adv Eng Softw 2002;33:227–42.
[9] Bonet JL, Romero ML, Miguel PF, Fernandez MA. A fast stress integration algorithm for reinforced concrete sections with axial loads and biaxial bending. Comput Struct 2004;82:213–25.
[10] Alfano G, Marmo F, Rosati L. An unconditionally convergent algorithm for the evaluation ofn the ultimate limit state of RC sections subject to axial force and biaxial bending. Internat J Numer Methods Engrg 2007;72(8):924–63.
[11] Rosati L, Marmo F, Serpieri R. Enhanced solution strategies for the ultimate strength analysis of composite steel–concrete sections subject to axial force and biaxial bending. Comput Methods Appl Mech Engrg 2008;197(9–12):1033–55.
[12] Cedolin L, Cusatis G, Ecchelli S, Roveda M. Capacity of rectangular cross-sections under biaxially eccentric loads. ACI Struct J 2008;105(2):215–24.
[13] Charalampakis AE, Koumousis VK. Ultimate strength analysis of composite sections under biaxial bending and axial load. Adv Eng Struct 2008;39(11):923–36.
[14] Eggert GM, Dawson PR, Mathur KK. An adaptive descent method for nonlinear viscoplasticity. Internat J Numer Methods Engrg 1991;31:1031–54.
[15] Crisfield MA. Non Linear Finite Element Analysis of Solids and Structures. Chichester: Wiley; 1991.
[16] Ramm E. Strategies for tracing the nonlinear response near limit points. In: Wunderlich W, Stein E, Bathe KJ, editors. Non-linear finite element analysis in structural mechanics. New York (NY): Springer-Verlag; 1981. p. 63–89.
[17] Lam WF, Morley CT. Arc-length method for passing limit points in structural calculation. J Struct Eng, ASCE 1992;118(1):169–85.
[18] Correa MR, Camotim D. On the arc-length and other quadratic control methods: established, less known and new implementation procedures. Comput Struct 2008;86(11–12):1353–68.
[19] Chiorean CG. A fast incremental-iterative procedure for inelastic analysis of RC cross-sections of arbitrary shape. Acta Tech Napocensis 2004;47:85–98.
[20] Zupan D, Saje M. Analytical integration of stress field and tangent material moduli over concrete cross-sections. Comput Struct 2005;83:2368–80.
[21] Roik K, Bergmann R. Composite columns-design and examples for construction. In: Roeder CW, editor. Composite and Mixed Construction. New York: ASCE; 1985. p. 267–78.